Available online at www.sciencedirect.com

ScienceDirect

Advances in Space Research xxx (2020) xxx–xxx

ADVANCES IN SPACE RESEARCH (a COSPAR publication)

www.elsevier.com/locate/asr

Geologic context and potential EVA targets at the lunar south pole

A.J. Gawronska [a,*], N. Barrett [b], S.J. Boazman [c,d], C.M. Gilmour [e], S.H. Halim [f], Harish [g], K. McCanaan [h], A.V. Satyakumar [i], J. Shah [j,k], H.M. Meyer [l,1], D.A. Kring [l,m]

[a] Department of Geology and Environmental Earth Science, Miami University, Oxford, Ohio, USA
[b] Department of Earth and Atmospheric Sciences, University of Alberta, Edmonton, Alberta, Canada
[c] Department of Earth Sciences, Natural History Museum, London, UK
[d] Department of Earth Sciences, University College London, London, UK
[e] Centre for Research in Earth and Space Science, York University, Toronto, Ontario, Canada
[f] Department of Earth and Planetary Sciences, Birkbeck, University of London, London, UK
[g] Planetary Sciences Division, Physical Research Laboratory, Ahmedabad, India
[h] School of Earth and Environmental Sciences, University of Manchester, Manchester, UK
[i] CSIR – National Geophysical Research Institute (CSIR-NGRI), Hyderabad, India
[j] Department of Earth Sciences, University of Western Ontario, London, Ontario, Canada
[k] The Institute for Earth and Space Exploration, University of Western Ontario, London, Ontario, Canada
[l] Lunar and Planetary Institute, Universities Space Research Association, Houston, Texas, USA
[m] NASA Solar System Exploration Research Virtual Institute, Mountain View, California, USA

Received 29 March 2020; received in revised form 22 May 2020; accepted 25 May 2020

Abstract

The lunar south pole is being targeted for exploration, in part, because it contains topographical high points with >50% illumination needed for solar power. Additionally, the south pole is being targeted because it contains permanently shadowed regions (PSRs), which may sequester resources in the form of volatile materials. Geologically, the pole lies on the rim of ~21 km diameter Shackleton crater, which is located on the topographic rim of the ~2,500 km diameter South Pole-Aitken (SPA) basin, the largest and oldest basin on the Moon. To prepare for future missions, we conducted a photogeologic analysis of the walls, rim, and ejecta of Shackleton crater. Two types of underlying (target) terrains were identified. The impact penetrated and exposed (1) purest anorthosite (PAN) representative of primitive crust and (2) a layered terrain that is likely a series of impact ejecta deposits that stratigraphically cover the crystalline crust. Crew performing extravehicular activities (EVAs) near the south pole may be able to sample PAN; impact melt from Shackleton, SPA, and other pre-Nectarian and Nectarian-age impacts; and polar regolith, including material from small PSRs that may contain volatile components. The topography in the south polar region is dramatic, often producing slopes in excess of 15°, creating mobility challenges for astronauts during EVAs.

Keywords: Extravehicular activity; Sample collection; Purest anorthosite; Ejecta layering; Slope constraints; Shackleton crater

* Corresponding author.
E-mail addresses: gawronaj@miamioh.edu (A.J. Gawronska), nbarrett@ualberta.ca (N. Barrett), s.boazman@nhm.ac.uk (S.J. Boazman), cgilmour@yorku.ca (C.M. Gilmour), shalim03@mail.bbk.ac.uk (S.H. Halim), harishnandal77@gmail.com (Harish), kathryn.mccanaan@manchester.ac.uk (K. McCanaan), satyageo41@gmail.com (A.V. Satyakumar), jshah68@uwo.ca (J. Shah), Heather.meyer@jhuapl.edu (H.M. Meyer), Kring@lpi.usra.edu (D.A. Kring).
[1] Current address: Applied Physics Laboratory, Johns Hopkins University, Laurel, Maryland, USA.

https://doi.org/10.1016/j.asr.2020.05.035
0273-1177/

1. Introduction

The National Aeronautics and Space Administration (NASA) has developed the Artemis program, consisting of a series of missions that include a human landing at the lunar south pole as early as 2024 (Bridenstine, 2019; Landau, 2019). The south pole is being targeted, in part, because it contains topographically high locations (Fig. 1), which provide >50% illumination needed for solar power (Fig. 2; Gläser et al., 2014; Mazarico et al., 2011; Speyerer and Robinson, 2013). The south pole is also being targeted because it contains permanently shadowed regions (PSRs) that may contain volatile elements in the form of ices suitable for in situ resource utilization (ISRU) (Anand, 2010; Anand et al., 2012; Duke et al., 2003; Fegley and Swindle, 1993; Spudis, 2011; Spudis and Lavoie, 2010). Access to those volatiles as well as underlying geologic samples will allow several scientific objectives to be addressed, as described in greater detail below.

The south pole is located on the rim of the 21 km diameter and 4.1 km deep Shackleton crater (Fig. 1). The rim of Shackleton crater was targeted as a landing site during the Constellation Program (Connolly, 2006; Gruener, 2009; NASA, 2007). Although the precise location of Artemis' landing has not yet been determined, the south polar region is rich with opportunities (e.g., Basilevsky et al., 2019; Flahaut et al., 2020; Lemelin et al., 2014; Lewis et al., 2019). The Artemis human landing system concept of operations is initially limited to two astronauts who land "on the lunar south pole" and will not exceed a surface stay of 6.5 days near the south pole (NASA, 2019a). Potentially, five extravehicular activities (EVAs) are possible in that interval (NASA, 2019b). Landing, traverses by crew and supporting robotic assets, and targeted sampling of the region require pre-mission geologic assessments of the lunar south pole. Here, we provide an initial geologic assessment of the lunar south pole, Shackleton crater, and the geology that may be accessible in that type of short duration surface stay.

1.1. Scientific motivation and objectives

A south pole landing is largely driven by operational issues related to solar power and volatile resources that may facilitate a sustainable exploration program. Access to the lunar surface will also provide an opportunity to address science objectives that are broadly recognized as important by the international community (e.g., The National Research Council (NRC), 2007; Crawford, 2015; Jawin et al. 2019; Pieters et al., 2018). One of those reports (NRC, 2007) identified eight concepts to be explored in future lunar missions. Among them is Concept

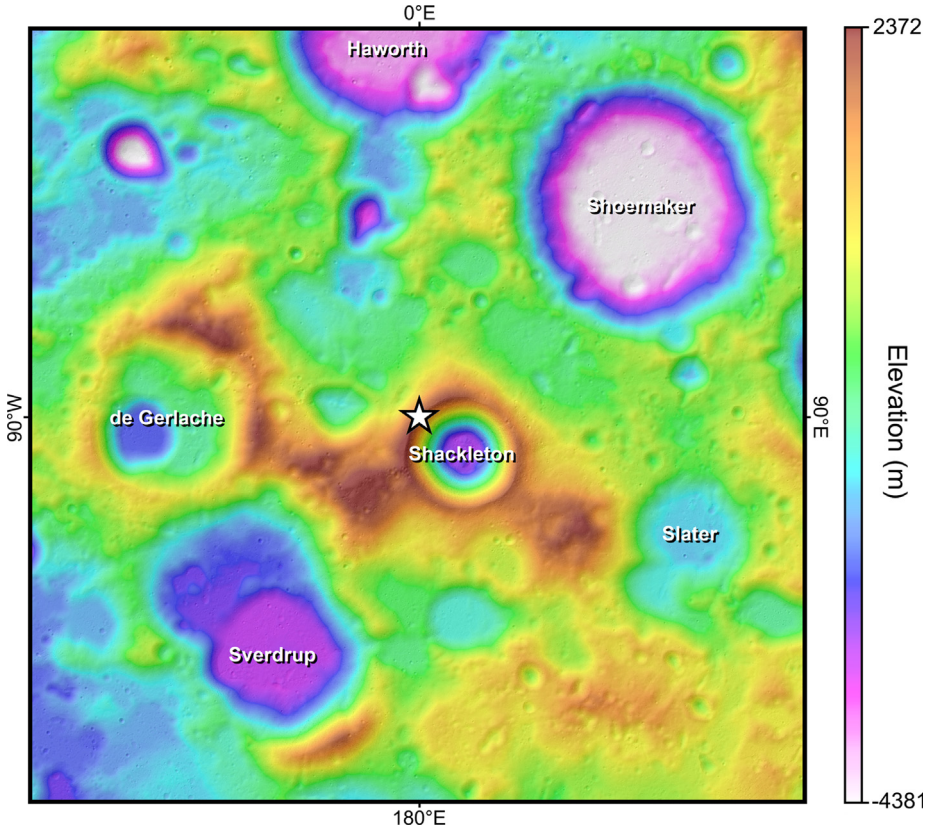

Fig. 1. Regional topographic map of the south polar region (LOLA DEM at 5 m/pixel) overlaid on hillshade. Labels indicate the location of Shackleton and other nearby craters. The white star denotes the location of the south pole. Note that Shackleton lies on a massif. The scale of this image is 1:600,000 – this scale is true at the south pole.

Please cite this article as: A. J. Gawronska, N. Barrett, S. J. Boazman et al., Geologic context and potential EVA targets at the lunar south pole, Advances in Space Research, https://doi.org/10.1016/j.asr.2020.05.035

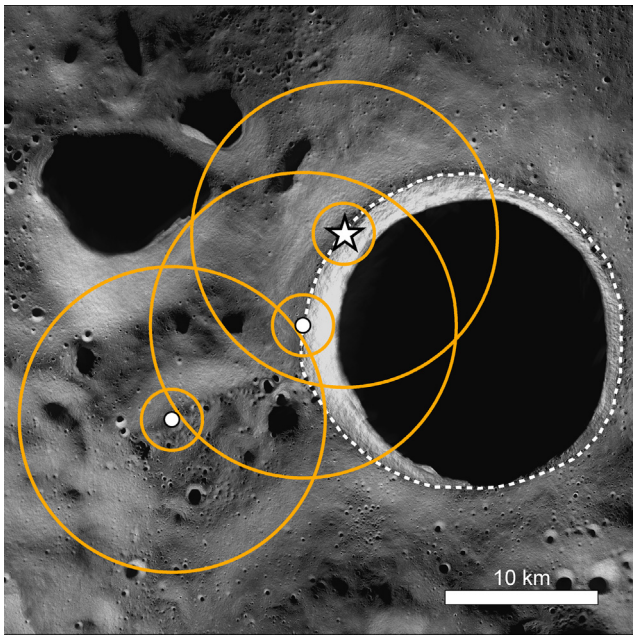

Fig. 2. Averaged NAC mosaic (map assembled by Arizona State University and downloaded from *Moon Trek*, Day and Law, 2018) outlining 2 km and 10 km exploration zones around the south pole (white star) and two points of highest illumination (white circles): one on the rim of Shackleton (89.78°S, 155.73°W) and one on the ridge connecting Shackleton and de Gerlache craters (89.45°S, 137.31°W) (Mazarico et al., 2011). Dashed white line represents Shackleton crater rim.

4, which states "The lunar poles are special environments that may bear witness to the volatile flux over the latter part of solar system history." This concept envisions investigations that analyze the composition of volatiles that may exist at the poles, as well as their source, alteration, transport, and retention. The concept additionally addresses the study of cold regolith, whether volatiles are preserved within the regolith, and what implications this has for the ancient lunar environment. Water ice deposits are of special interest for lunar ISRU efforts, because they can be processed into the resources that are necessary to establish a sustainable space exploration program (e.g., propellant, oxygen, potable water) (Anand, 2010; Anand et al., 2012; Duke et al., 2003; Spudis, 2011; Spudis and Lavoie, 2010). As suggested by (1) the Diviner Lunar Radiometer Experiment (DLRE; Paige et al., 2010), (2) the Lunar Exploration Neutron Detector (LEND; Mitrofanov et al., 2010a), and (3) the Lyman Alpha Mapping Project (LAMP; Gladstone et al., 2010), all onboard NASA's Lunar Reconnaissance Orbiter (LRO; Chin et al., 2007), water ice exists at the lunar poles, and it is likely that other volatiles are also present in polar cold traps (Colaprete et al., 2010; Fisher et al., 2017; Gladstone et al., 2012; Haruyama et al., 2008; Hayne et al., 2015; Mandt et al., 2016; Mazarico et al., 2011; Miller et al., 2014; Mitrofanov et al., 2010b; Paige et al., 2010; Schultz et al., 2010; Siegler et al., 2015). Furthermore, volatiles are likely to be concentrated in PSRs located near the lunar poles due to their stable and extremely cold thermal environments (Arnold, 1979; Feldman et al., 2001; Gladstone et al., 2012; Hayne et al., 2015; Lawrence, 2016; Lemelin et al., 2014; Li et al., 2018; Spudis et al., 2008; Watson et al., 1961). Any ice in the south polar region likely exists in the form of regolith-ice mixtures (Campbell et al., 2006; Nozette et al., 2001; Thomson et al., 2012). Sampling of regolith near and within PSRs close to the lunar south pole would address questions about the origin and extent of volatile deposits (e.g., Cisneros et al., 2018; Lemelin et al., 2014).

The geologic history of the lunar south pole region is shaped by the creation of the immense (2,500 km diameter) and ancient (3.9 to –4.3 Ga) South Pole-Aitken (SPA) basin (Fassett and Minton, 2013; Hiesinger et al., 2011, 2012; Morbidelli et al., 2012; Potter et al., 2012; Spudis et al., 2008; Stöffler et al., 2006). The SPA basin is a deep depression that extends to a depth of 13.5 km (James et al., 2019; Potter et al., 2012; Smith et al., 2010) within which Shackleton lies. Thus far, samples from the lunar far side have not been collected, and major geologic events, including the timing of a hypothesized lunar cataclysm relative to that of the SPA impact, remain poorly understood (e.g., Chapman et al., 2007; Cohen et al., 2000; Ćuk, 2012; Fassett and Minton, 2013; Fassett et al., 2012; Hartmann, 2003, 2019; Hurwitz and Kring, 2015; Marchi et al., 2012; Morbidelli et al., 2012; Potter et al., 2012; Ryder, 2000; Tera et al., 1974). Because Shackleton lies along the margin of the SPA basin, sampling materials such as the rock exposures and boulders found within Shackleton's ejecta may answer additional questions about SPA basin and other initiatives outlined by the NRC (2007) (i.e., concepts 1, 3, 6, 7, 8).

1.2. Shackleton crater and the south pole region

Shackleton is a well-preserved simple crater (e.g., Spudis et al., 2008; Zuber et al., 2012). This 21 km diameter crater was initially assigned an Eratosthenian age (1.1 to 3.2 Ga; Wilhelms, 1987; Wilhelms et al., 1979), and is labeled as such in the recent Unified Geologic Map of the Moon (Fortezzo et al., 2020), although several assessments of the impact modification of Shackleton suggest an age between 3.51 and 3.69 Ga (Spudis et al., 2008; Tye et al., 2015; Zuber et al., 2012). Shackleton is significantly younger than several neighboring craters: Haworth (4.18 ± 0.02 Ga), Shoemaker (4.15 ± 0.02 Ga), and Faustini (4.10 ± 0.03 Ga) (Tye et al., 2015). Shackleton was excavated, in part, from a preexisting, irregular massif, resulting in a tilting of the crater rim with a downward slope towards the eastern lunar near side. This massif is a prominent feature in the lunar south polar region (Stopar and Meyer, 2019) and connects Shackleton to de Gerlache crater ("Connecting Ridge" described in detail by Gläser et al., 2014). Spudis et al. (2008) infer that the age of this ridge is similar to the age of the nearby pre-Nectarian de Gerlache crater. This massif rises to a maximum elevation of ~1900 m while the elevation of Shackleton's rim ranges

Please cite this article as: A. J. Gawronska, N. Barrett, S. J. Boazman et al., Geologic context and potential EVA targets at the lunar south pole, Advances in Space Research, https://doi.org/10.1016/j.asr.2020.05.035

from ~900 m to ~1760 m. The south pole on the rim of Shackleton has an elevation of 1290 m. The massif coincides with several other massifs along the southern topographic margin of the SPA basin and, thus, Spudis et al. (2008) infer that the massif is a product of the SPA basin-forming impact event.

The Shackleton impact event exposed blocks of ancient crustal material, including what is believed to be purest anorthosite (PAN) in its crater walls (Yamamoto et al., 2012). This lithology has an estimated >98% modal plagioclase feldspar abundance (Ohtake et al., 2009). The extent of PAN throughout the lunar crust is debated (Lemelin et al., 2015; Nagaoka et al., 2014; Ohtake et al., 2009) and is difficult to estimate based on current lunar chemical differentiation models involving a magma ocean (Longhi, 2003; Wieczorek et al., 2006). PAN may exist as small clasts within meteorites (e.g., Nagaoka et al., 2014), but no significant samples of PAN have been identified in the Apollo collection. If blocks of exposed PAN can be located within the Shackleton ejecta, that will greatly improve our understanding of the origin of PAN in the lunar crust, the production of massifs by the SPA basin-forming impact, and the subsequent geologic evolution of the region.

2. Data and methods

2.1. Datasets and image processing

Datasets from the LRO (Chin et al., 2007), namely the Lunar Orbiter Laser Altimeter (LOLA) (Smith et al., 2010) and LRO Camera (LROC) Narrow Angle Cameras (NACs) (Robinson et al., 2010), were used for topographic analysis and photogeologic interpretation of a 20 km^2 area within the south polar region (centered on the south pole, Fig. 2). A LOLA 5 m/pixel digital elevation model (DEM) with a corrected scaling factor was used to create a topography map of the south polar region (Fig. 1). LOLA-derived hillshade and slope maps were derived using Raster Surface 3D analyst tools in ArcMap ("Hillshade" and "Slope," respectively; ArcGIS software). LRO NAC images with ~0.5 to 1.2 m/pixel resolution and ~87° to 91° incidence angles were used for detailed mapping of outcrop-scale (~2 m) features. The images were processed and projected to a lunar polar stereographic projection using the United States Geological Survey (USGS) digital image processing software, Integrated Software for Imagers and Spectrometers 3 (ISIS3; e.g., Edmundson et al., 2012; Edwards, 1987; Torson, 1989).

2.2. Identification of geologic features

This study is focused on geologic features with sampling potential during EVA. Targets include rock exposures and associated boulders, as well as fresh craters. Boulders are recognizable as bright, positive relief features that are most easily identified by their shadows. Rock exposures are also generally composed of high albedo material, surrounded by lower albedo material (regolith). Craters are identified as bowl-shaped depressions, with half of their wall exposed by incoming sunlight, resulting in a shadow on the opposite half of the crater. Craters with high albedo ejecta and an uplifted rim (i.e., younger craters; Daubar et al., 2014; Moore et al., 1980; Thompson et al., 1974) and craters with associated boulders were mapped separately from older, more subdued craters because such fresh craters have the best sampling potential. Additionally, NAC images were used to investigate geologic features in the exposed walls of Shackleton crater; for example, PAN locations of Yamamoto et al. (2012) were correlated with NAC imagery to investigate the nature of any PAN exposures. Identified PAN exposures are of high albedo; boulders with similar albedo compositions were mapped in the Shackleton ejecta and, at least in some cases, likely represent ejected pieces of PAN.

2.3. Topographic constraints on EVAs

Features that may be sampled during an EVA are bound by the range and slope limits of the deployed mission to ensure the safety of the crew. Unassisted EVAs may be limited to a 2 km exploration zone on terrains with slopes <15° (Allender et al., 2019; Öhman and Kring, 2012). This may be expanded to 10 km and 25°, respectively, if a pressurized rover is utilized (Allender et al., 2019; Öhman and Kring, 2012). We document examples of geologic features for EVA targets within 2 and 10 km radially from the lunar south pole (Fig. 2). In addition, to maintain crew safety, we recognize the rim crest of the Shackleton crater as another boundary to exclude possible EVA targets that would be on a downward-facing slope towards the interior of the crater. Note that the south pole is located on the inside of our rim crest limit. We additionally describe features within 10 km of a point of highest illumination on the rim of Shackleton identified by Mazarico et al. (2011), although the 10 km zones surrounding the south pole and this illumination point overlap (Fig. 2). To further assist in selecting EVA targets, a map of PSRs in the region, as well as slope profiles along a traverse for both the ridge and rim of Shackleton crater, were created. Mean slope values along the profile were calculated at user defined breaks (e.g., every time the slope changed by >2°), providing additional information on the topography that may be encountered during EVA. To generate the PSR map, a LOLA data product showing PSRs in the south polar region was overlaid on a NAC mosaic. This product is available through the LOLA Planetary Data Systems (PDS) Data Node (LOLA PDS Data Node LPSR-85S-60 M-201608.JP2).

3. Results and discussion

We begin with a geologic assessment of Shackleton crater and potential scientific and exploration targets in the vicinity of the lunar south pole. This assessment extracts

Please cite this article as: A. J. Gawronska, N. Barrett, S. J. Boazman et al., Geologic context and potential EVA targets at the lunar south pole, Advances in Space Research, https://doi.org/10.1016/j.asr.2020.05.035

geologic context from exposures in Shackleton crater walls (Section 3.1) and in debris ejected by the Shackleton impact (Section 3.2). We also present an examination of potential sampling locations with respect to PSRs (Section 3.3). We then examine the accessibility of those sites within the limits of topography and slope (Section 3.4).

3.1. Geologic context: The inner walls of Shackleton

Shackleton crater lies on the edge of the SPA basin and, thus, the target material is expected to be mostly composed of ancient noritic crust seen elsewhere in this region (Borst et al., 2012; Hurwitz and Kring, 2015; Moriarty and Pieters, 2018; Pieters et al., 1997, 2001; Vaughan and Head, 2014). This noritic material may be exposed within the crater walls, although more work is needed to confirm this. A previous analysis of spectral reflectance data in Shackleton crater suggests the presence of PAN in the crater walls (Yamamoto et al., 2012). Here, we correlated the locations of the previously measured PAN spectra with NAC images and found that large rocky exposures of PAN (e.g., Fig. 3b-c) are located just below the crater rim, down to a depth of approximately 900 m, beyond which the crater wall is obscured by permanent shadow. The PAN exposures were excavated by the Shackleton impact, thus indicating that the original target terrain underlying the lunar geographic south pole, and extending into the massif, is composed, at least in part, of PAN. The PAN could be intact crystalline crust or potentially part of a megabreccia with ~100-m-scale blocks. We note that low albedo regolith is sporadically identified throughout the exposures and appears to form downslope streamers that may reflect mass wasting towards the crater floor (Fig. 3d). We cannot ascertain whether the lower albedo material is continuous with the PAN (and, thus, part of a crystalline crust) or interstitial to the PAN (and, thus, a second lithological component in a megabreccia). We find no evidence of cryptic layering within the PAN-bearing blocks; however, we are limited by the resolution of the images to features ~2 m or greater in scale. It is possible that the massif cross-cut by Shackleton crater is composed of different, non-PAN material, but the underlying rock is covered by loose debris due to mass wasting and, thus, not discernable. Likewise, the permanently shadowed crater walls prevent any photogeologic assessment of the underlying material.

The nature of the crater wall is very different on the side opposite to the south pole. There, a layered terrain is exposed (Fig. 3e). Individual layers in the sequence are approximately 10 to 50 m thick and the complete sequence varies between 100 and 200 m thick vertically. The sequence begins approximately 10 m below the rim, but the lateral extent of these layers is difficult to determine based on currently available NAC images with suitable illumination (~87° to 91° incidence). A potentially useful analogue for such layered sequences is Meteor Crater, a terrestrial impact crater with the same simple crater morphology as Shackleton and in a layered terrain. In situ studies indicate the layered sequence in the walls of Meteor Crater represent uplifted target strata and overturned strata in the ejecta deposit that forms the uppermost crater rim (e.g., Kring, 2007, 2017). If the layered units at Shackleton are pre-existing target strata, then those layers likely represent impact ejecta horizons deposited by older impact events, such as those that produced the Haworth, Shoemaker, and Faustini craters. Alternatively, one or more layers in the uppermost portion of Shackleton's walls could have been produced from ejecta of the Shackleton impact event. Based on a computer simulation of the Shackleton impact event (Halim et al., under review), >150 m of ejecta is anticipated on the crater rim. There is no evidence of volcanism in the region and, thus, layered volcanic lava flows are ruled out as a source for the layers.

To evaluate the possibility that the layers may be ejecta deposits from older impact events, the thicknesses of ejecta produced by nearby craters were calculated using scaling laws appropriate for complex craters (e.g., Kring, 1995), akin to the types of craters in the south polar region that could have produced appropriately-thick layers in Shackleton. Measurements of crater diameters and distances were acquired using QuickMap developed by the LROC team. Craters examined were, in approximate stratigraphic order from oldest to youngest (Deutsch et al., 2020; Tye et al., 2015), Amundsen-Ganswindt, Schrödinger, an unnamed crater between Sverdrup and Wiechert J, an unnamed crater adjacent to de Gerlache, Haworth, Shoemaker, Faustini, Amundsen, de Gerlache, Nobile, Slater, Sverdrup, and Cabeus. Calculated ejecta thicknesses corresponding to the layered deposits in the Shackleton wall (Fig. 3e) range from 399 to 537 m (from the Amundsen-Ganswindt basin) to <10 m (from Sverdrup and Slater) (Table 1). The youngest craters would have produced layers towards the top of the Shackleton target region: e.g., Amundsen (9 to 26 m), de Gerlache (1 to 6 m), Nobile (4 to 14 m), Slater (4 to 11 m), Sverdrup (3 to 11 m), and Cabeus (4 to 14 m). The older, larger basins may have produced deeper layers, now hidden within the PSR of Shackleton crater. Based on revised ages for the region's craters, Faustini, Haworth, and Shoemaker have pre-Nectarian ages (Tye et al., 2015), and Amundsen and Schrödinger basin have Nectarian ages (Wilhelms et al., 1979). It is important to note that some of the ejecta from those craters may have landed with sufficient speed to mix with underlying surface materials via ballistic sedimentation (Oberbeck, 1975). That process would thicken an overlying layer at the expense of an underlying layer. Using the ballistic formula for crater ejecta (Oberbeck, 1975), impact speeds at the location of the Shackleton layered deposits were on the order of 1000 km/hr (Table 1).

3.2. Potential EVA targets in Shackleton crater ejecta

Thousands of boulders are scattered throughout the ejecta of Shackleton in the vicinity of the south pole

Please cite this article as: A. J. Gawronska, N. Barrett, S. J. Boazman et al., Geologic context and potential EVA targets at the lunar south pole, Advances in Space Research, https://doi.org/10.1016/j.asr.2020.05.035

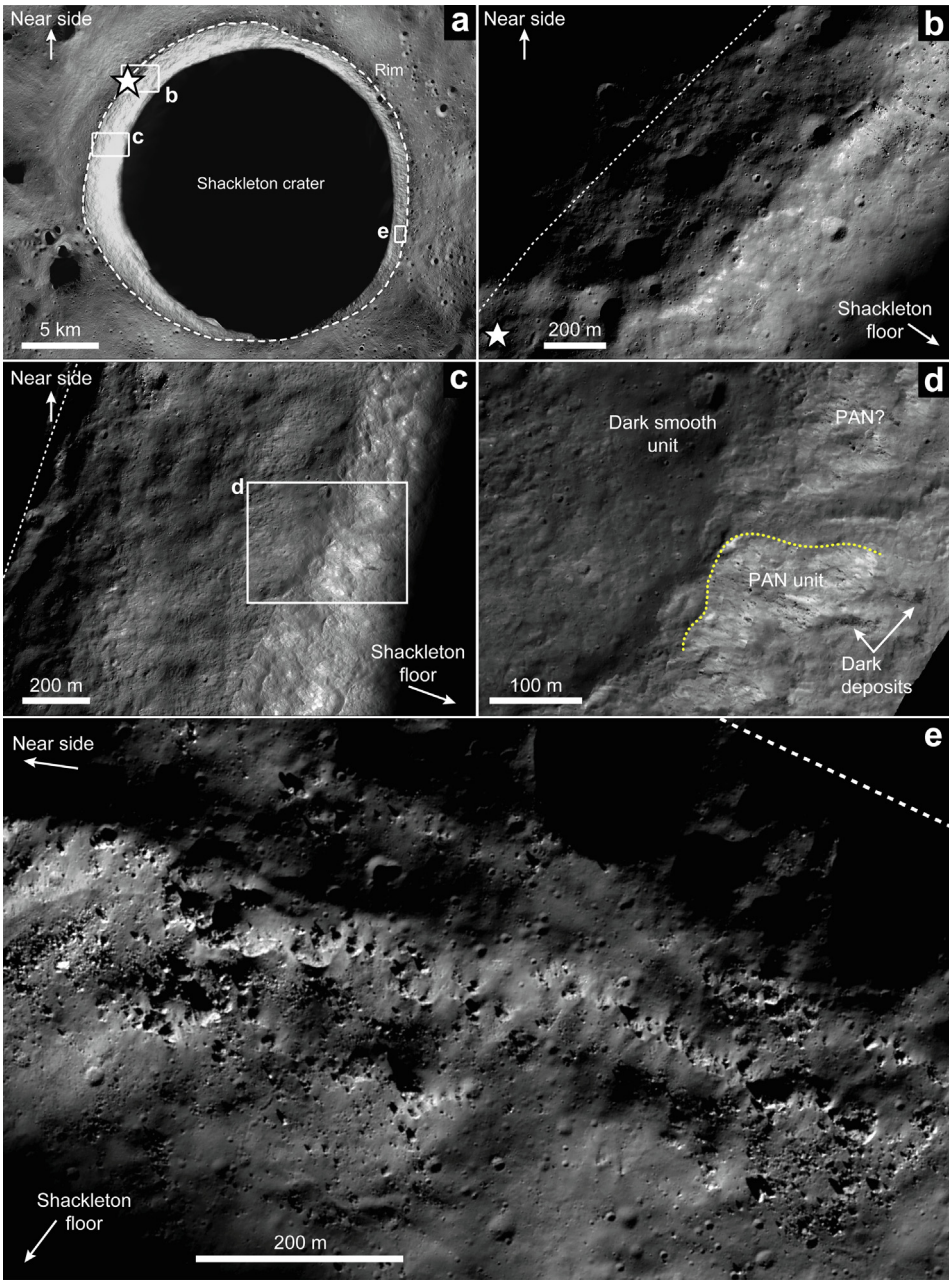

Fig. 3. **(a)** Averaged NAC mosaic (downloaded from *Moon Trek*, Day and Law, 2018) showing the locations of images **b**, **c**, and **e**. The location of image **d** is shown in image **c**. The south pole is denoted by the white star. **(b)** Detail of NAC M133786042L showing the bright rock exposure of PAN identified in Yamamoto et al. (2012). These PAN rock exposures are ~500 m from the south pole. **(c)** Detail of NAC M146833333L and M133786042L (stitched together) showing blocks of PAN >500 m wide. The white box shows the location of image **d**. **(d)** A close-up image of the crater wall. Detail of NAC M133786042L reveals dark material along PAN deposits. **(e)** Detail of NAC M133154995L (rotated 80° CCW) highlighting the layered stratigraphy in the inner wall of Shackleton crater opposite to the south pole.

(Figs. 4–6). Boulder fields in our survey region appear mostly associated with small, relatively fresh craters in the Shackleton ejecta deposit (e.g., Figs. 4d-e, -h, 5h-i). Identifying specific features within boulders (i.e., layers, fractures, tracks, etc.) was a challenge given the high angle of solar incidence. Due to the resolution of the NAC images compared to boulder size, boulder albedo was relied upon to make inferences about the Shackleton region. Most boulders near to the south pole exhibit a high albedo (e.g., Fig. 4d) and may be fragments of ejected crystalline crustal lithology (potentially PAN), suitable for sampling. Some boulders identified are of low albedo (e.g., Fig. 5i), providing evidence of heterogeneous material ejected during Shackleton's formation. Spectra of boulders were not reported by Yamamoto et al. (2012), probably due to their small size relative to the size of the spectral footprint. Additionally, because the low sun angle produces low signal-to-noise levels, and the boulders are small relative to the res-

Please cite this article as: A. J. Gawronska, N. Barrett, S. J. Boazman et al., Geologic context and potential EVA targets at the lunar south pole, Advances in Space Research, https://doi.org/10.1016/j.asr.2020.05.035

Table 1
Calculated thicknesses and velocities of ejecta deposits corresponding to nearby craters that could have produced the layered deposits in the wall of Shackleton.

*Crater name**	*Crater diameter (m)***	*Crater radius (m)***	*Distance to point (m)****	*Calculated ejecta thickness (m) for range of exponents*			*Maximum flight time (s)*****	*Maximum velocity (km/s)*****	*Maximum velocity (km/hr)*****
				−3.5	*−3*	*−2.5*			
Unnamed - between Sverdrup and Wiechert J	70640	35320	98000	9	15	25	347	0.3989	1436
Schrodinger basin	311985	155993	443000	25	43	72	739	0.8482	3053
Amundsen	100135	50068	152000	9	15	26	433	0.4968	1789
Faustini	39166	19583	68000	3	5	9	289	0.3323	1196
Shoemaker	50316	25158	60000	12	19	29	272	0.3122	1124
Haworth	53533	26766	92000	4	7	12	337	0.3865	1392
de Gerlache	31999	16000	64000	1	3	6	281	0.3224	1161
Unnamed - next to de Gerlache	37716	18858	53000	5	9	15	255	0.2934	1056
Sverdrup	32708	16354	51000	3	6	11	251	0.2878	1036
Cabeus	83906	41953	156000	4	7	14	438	0.5033	1812
Slater	23134	11567	32000	4	7	11	199	0.2280	821
Nobile	77537	38768	139000	4	8	14	414	0.4751	1710
Amundsen-Ganswindt basin	377977	188989	254000	399	463	537	559	0.6423	2312

* All craters exhibit complex morphology and exist within two diameters of Shackleton where layers are observed. These craters are listed from youngest to oldest based on approximate relative ages (after Deutsch et al. (2020) and Tye et al. (2015), and potentially represent stratigraphic order in the wall of Shackleton crater.
** Diameters and distances measured in LROC Quickmap (accessed September 26, 2019).
*** Based on distance from crater center to Shackleton layer location.
**** Velocity and flight time may also be affected by variable ejection angles.

Please cite this article as: A. J. Gawronska, N. Barrett, S. J. Boazman et al., Geologic context and potential EVA targets at the lunar south pole, Advances in Space Research, https://doi.org/10.1016/j.asr.2020.05.035

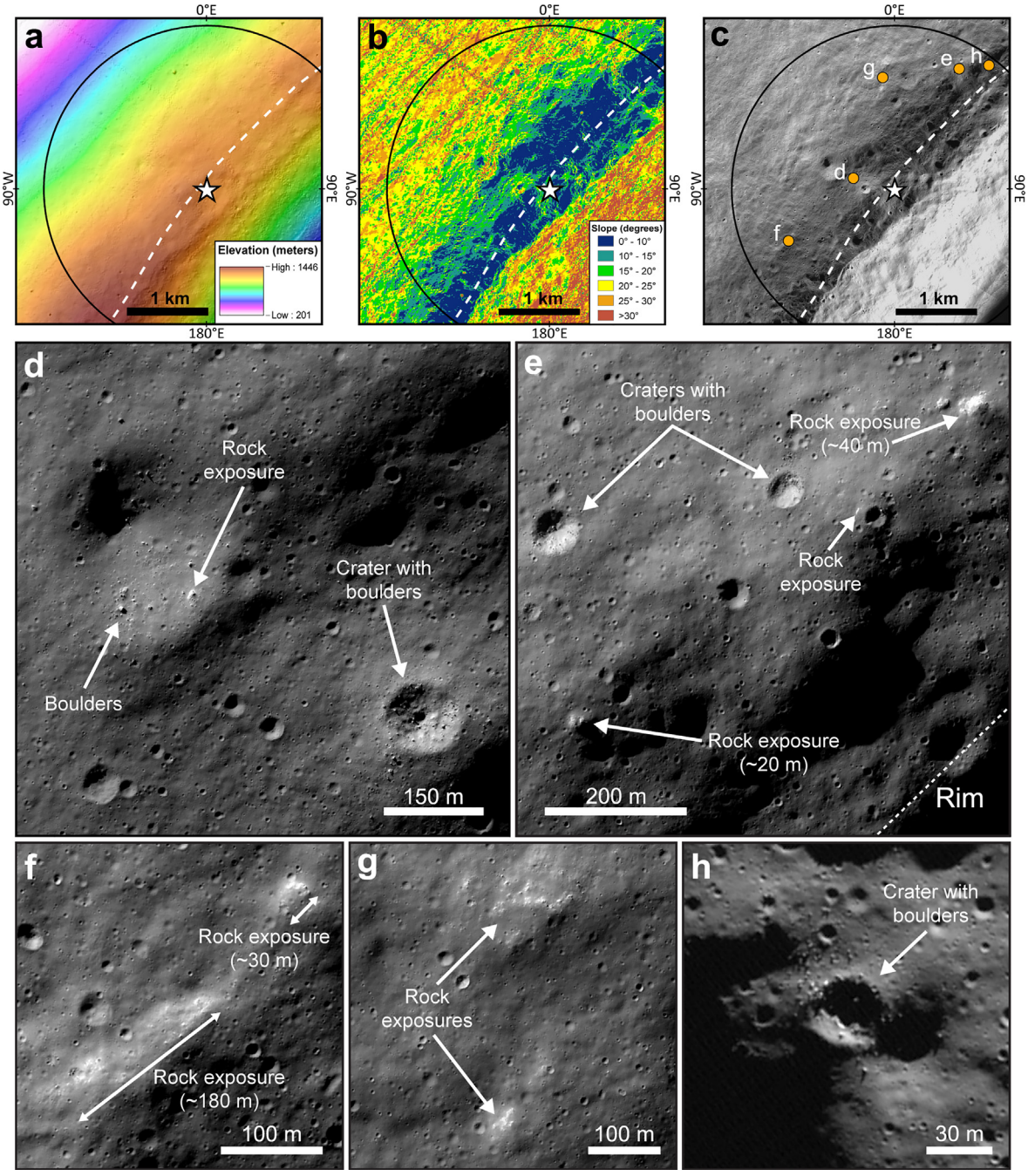

Fig. 4. Potential EVA targets in a 2 km exploration zone around the south pole. **(a)** LOLA DEM (5 m/pixel) overlaid on hillshade showing the topography within the 2 km boundary. **(b)** LOLA-derived slope map of the same extent. **(c)** Averaged NAC mosaic (downloaded from *Moon Trek*, Day and Law, 2018) showing the locations of annotated images **d** to **h**. Coordinates and associated NAC images of these locations can be found in Table A.1. Figures **d**, **e**, and **f** are on the edge of slopes >15° and may be inaccessible without rover assistance.

olution of both the Moon Mineralogy Mapper (~70 m, Goswami and Annadurai, 2009) and the Multiband Imager onboard the Selenological and Engineering Explorer (SELENE, also named Kaguya) (~20 m, Ohtake et al., 2008), spectral data has not been used to probe the compositions of the boulders. Recently, the identification of boulder tracks has become fundamental to our understanding of physical properties of the lunar regolith and trafficability (Bickel et al., 2019; Sargeant et al., 2019). Based on our analysis, boulder tracks appear to either be a rare feature on the ejecta deposit of Shackleton crater or are not easy to discern using the current resolution of available imagery. Where apparent, they appear to be produced by boulders ejected from craters.

Rock exposures from approximately 20 to 200 m in size are found throughout the ejecta in the EVA target boundaries (Figs. 4–6). These rock exposures are far more massive than most boulders sampled during Apollo (largest

Please cite this article as: A. J. Gawronska, N. Barrett, S. J. Boazman et al., Geologic context and potential EVA targets at the lunar south pole, Advances in Space Research, https://doi.org/10.1016/j.asr.2020.05.035

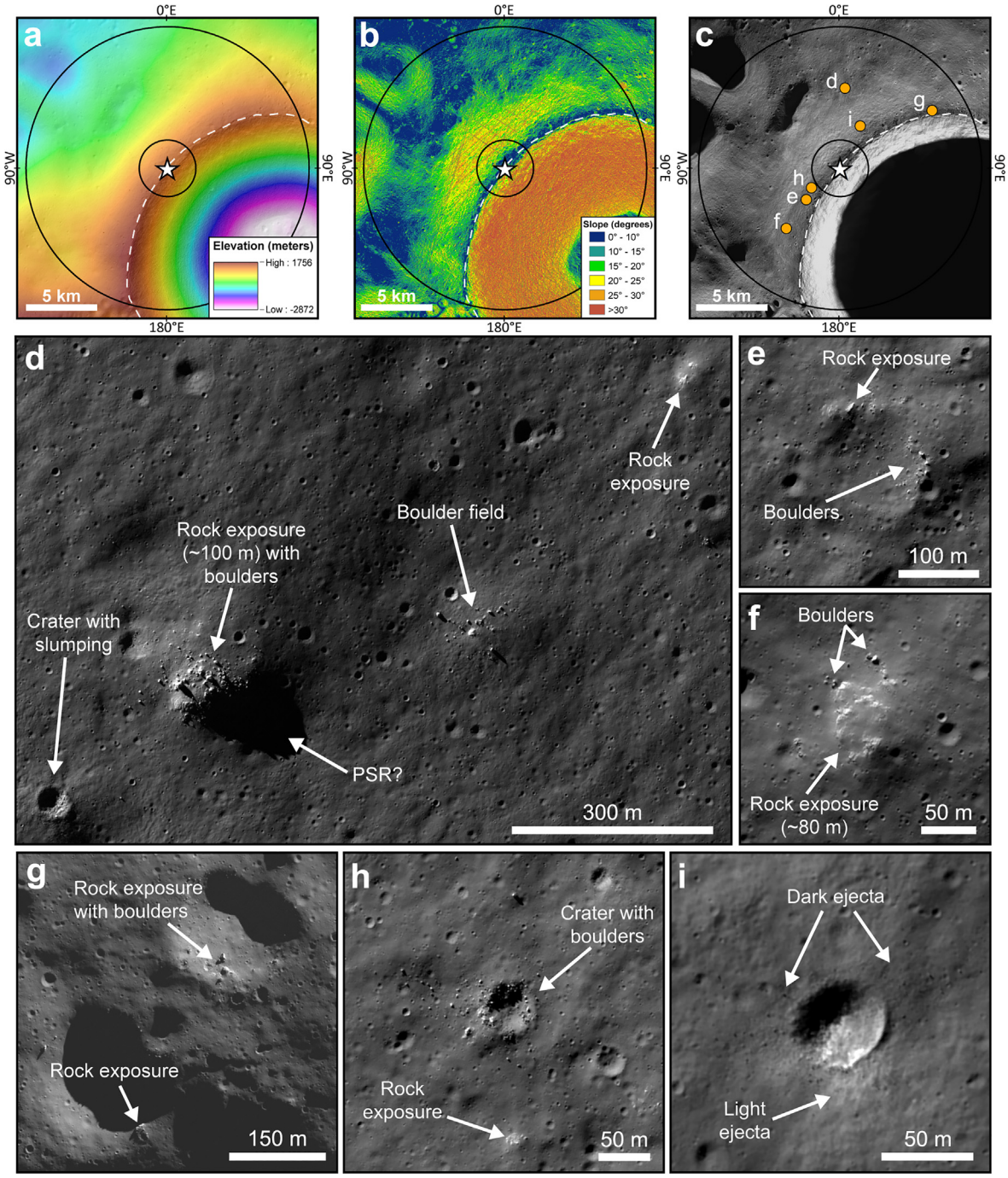

Fig. 5. Potential EVA targets in a 10 km exploration zone around the south pole. **(a)** LOLA DEM (5 m/pixel) overlaid on hillshade showing the topography within the 10 km boundary. **(b)** LOLA-derived slope map of the same extent. **(c)** Averaged NAC mosaic (downloaded from *Moon Trek*, Day and Law, 2018) showing the locations of annotated images **d** to **i**. Coordinates and associated NAC images of these locations can be found in Table A.1. A PSR may have been formed by the shadow of the rock exposure in **d**; however, this will have to be confirmed with illumination and temperature investigation of the area at higher resolution than currently available.

sampled boulders reached sizes of approximately 4 m; Spudis and Ryder, 1985; Swann et al., 1977; Ulrich et al., 1981; Wolfe et al., 1981), although the largest boulder ever approached reached a size comparable to the smallest exposures observed here ("House Rock," Apollo 16; Ulrich et al., 1981). Moreover, exposures identified here are on the scale of highway outcrops on Earth, which can provide tremendous insights to the geologic processes that produced a lithology, as well as how such lithologies may age on the Moon (i.e., Basilevsky et al., 2015). Studying the exposures, as well as sampling them, should be enlightening. In some cases, large rock exposures have fragmented into boulders (e.g., Figs. 5d, -f, 6d), which may give ease to sampling. The high albedo of the expo-

Please cite this article as: A. J. Gawronska, N. Barrett, S. J. Boazman et al., Geologic context and potential EVA targets at the lunar south pole, Advances in Space Research, https://doi.org/10.1016/j.asr.2020.05.035

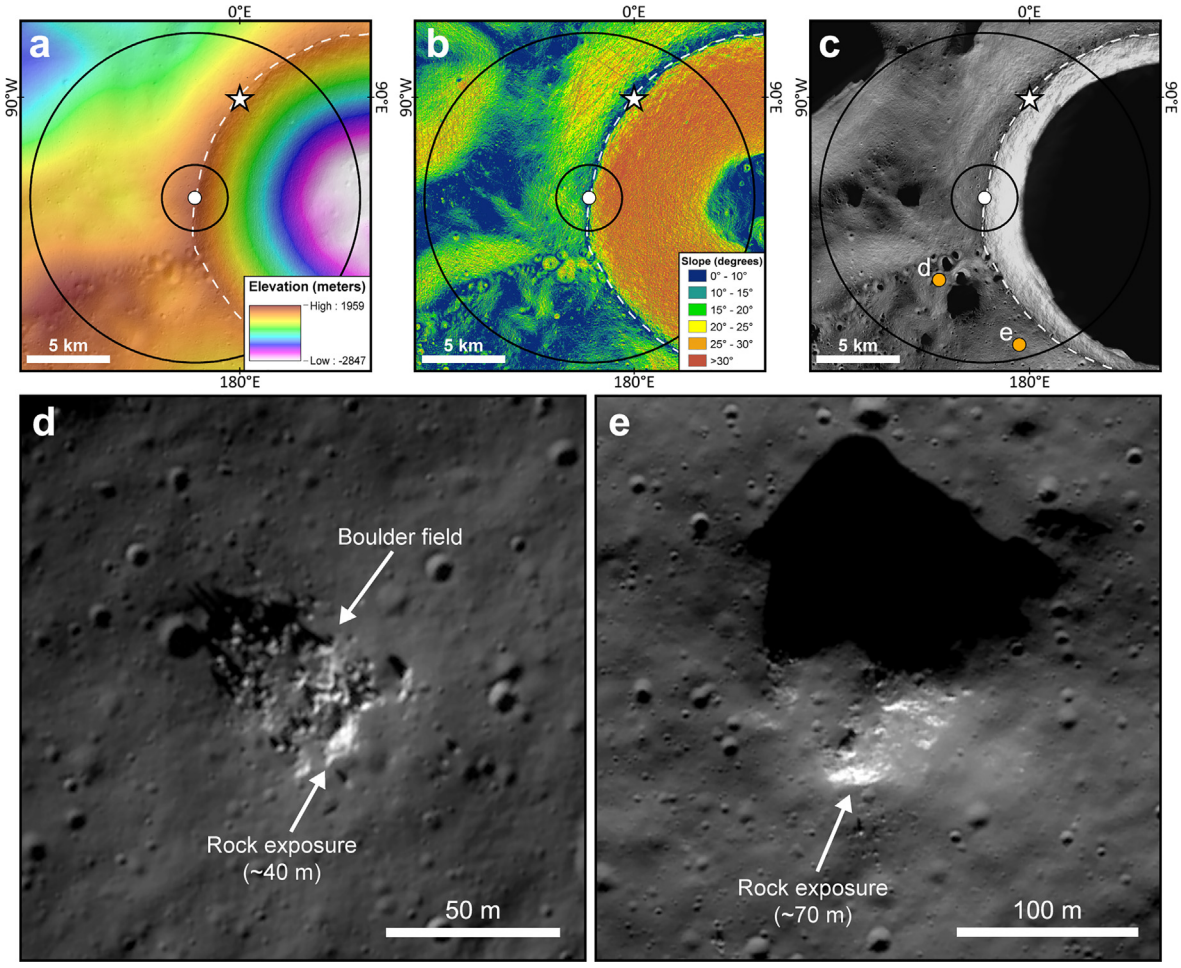

Fig. 6. Potential EVA targets in a 10 km exploration zone around the highest illumination point on the rim of Shackleton (89.78°S, 155.73°W). **(a)** LOLA DEM (5 m/pixel) overlaid on hillshade showing the topography within the 10 km boundary. **(b)** LOLA-derived slope map of the same extent. **(c)** Averaged NAC mosaic (downloaded from *Moon Trek,* Day and Law, 2018) showing the locations of images **d** and **e**. Coordinates and associated NAC images of these locations can be found in Table A.1. Most features in this region overlap with the region outlined in Fig. 5 – the two EVA targets in **d** and **e** do not. Image **(e)** does not preserve a PSR – the shadowed region seen here is due to high solar incidence angle.

sures suggests that they may represent the PAN lithology that was ejected either as large, individual blocksthat are partially covered by regolith, or, alternatively, small blocks that were deposited a similar distance from the rim. Because lithologies excavated from the deeper regions of a crater dominate the crater rim, the rocks nearest to the Shackleton rim may represent deeper crustal lithologies (e.g., norite, Borst et al., 2012; Kramer et al., 2013; Pieters et al., 2001).

Sampling small craters on the Shackleton ejecta deposit can provide information on the regional subterranean structure. During crater formation, material is exposed from below the lunar surface and is dispersed around the crater as part of an ejecta deposit (e.g., Fig. 5i). Craters of 5 to 150 m diameter, seen on the rim and flanks of Shackleton, can excavate material from depths of 1 to 30 m (Pike, 1974). Because the excavation depth values are less than the ~150 m thickness of Shackleton ejecta, the material should simply represent more deeply buried ejecta. However, if the target is layered, that layering may be discernable by sampling the overturned debris as a function of depth. We also note that this freshly excavated material often appears brighter than the surrounding materials (e.g., Fig. 5i), as exposure to space weathering causes older and undisturbed material to mature and darken over time (Gold, 1955; Thompson et. al., 1974). In addition to rock exposures, regolith samples near smaller craters in the Shackleton region would be of scientific value to study surface weathering processes on airless bodies (Noble et al., 2000).

3.3. Distribution of PSRs in the vicinity of the south pole

Investigating PSRs in the south polar region will help address questions regarding the composition, abundance, and distribution of lunar volatiles (e.g., Arnold, 1979; Feldman et al., 2001; Lemelin et al., 2014; Watson et al., 1961). PSRs of variable sizes are found throughout the Shackleton region (Fig. 7). The apparent field of PSRs precisely at the pole is largely a data artifact, as it does not

Please cite this article as: A. J. Gawronska, N. Barrett, S. J. Boazman et al., Geologic context and potential EVA targets at the lunar south pole, Advances in Space Research, https://doi.org/10.1016/j.asr.2020.05.035

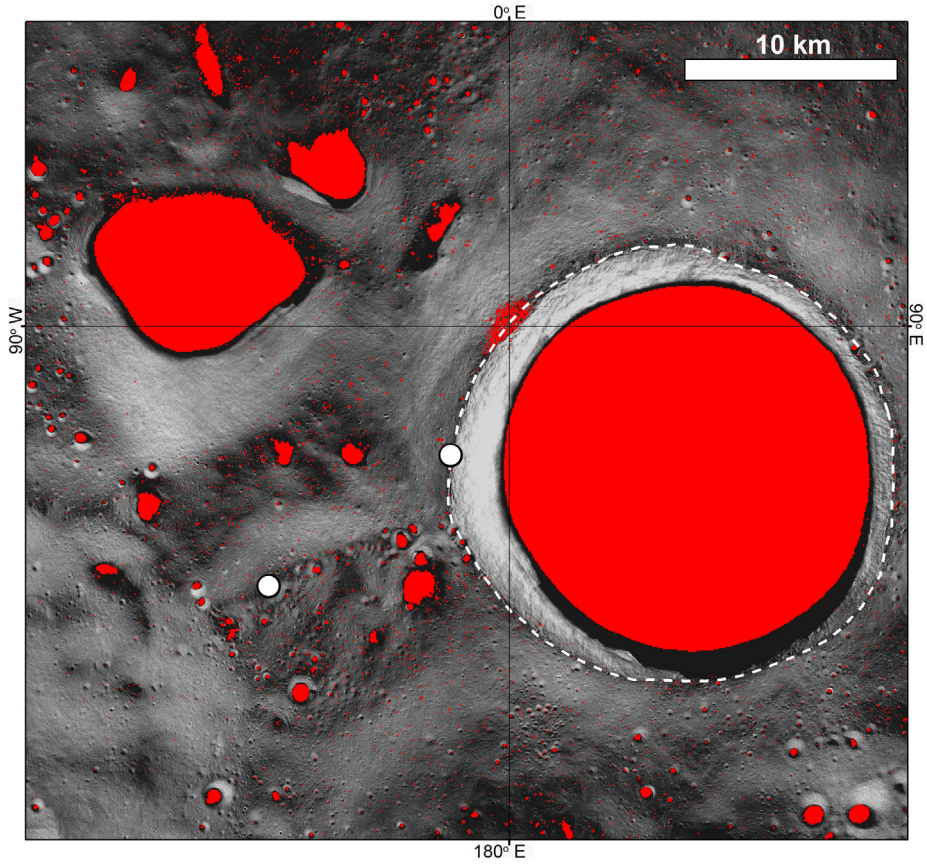

Fig. 7. LOLA PSR map (60 m/pixel) overlaid on NAC mosaic showing PSRs in the south polar region (LOLA PDS Data Node LPSR-85S-60M-201608. JP2). White dash line denotes the rim of Shackleton crater. White points mark the locations of two high illumination points identified by Mazarico et al. (2011). PSRs are denoted as red regions in this figure, with the exception of the south pole, which may be an artifact. (For interpretation of the references to colour in this figure legend, the reader is referred to the web version of this article.)

appear to correspond to identifiable PSRs in the high resolution LROC images of that area (e.g., Fig. 3b). Some sites near rock exposures may also preserve small PSRs, similar to the Apollo 16 "Shadow Rock" (Ulrich et al., 1981). Long-period temperature (i.e., LRO Diviner) and illumination (i.e., LOLA) data are needed to confirm where small PSRs exist; if confirmed, such locations will be an important EVA target for volatile investigations. However, considering the small size and likely young age of such smaller PSRs, any volatiles, if present, may only be products of solar wind implantation. Generally, the distribution of PSRs in the south polar region appears to correlate with craters. The age of these craters is important as it dictates the volatile composition (Kring, 2019). Craters with ages > 3.5 Ga (e.g., Cabeus, Haworth, Shoemaker, Faustini, de Gerlache, and Shackleton) may have accumulated volatiles from ancient impact events and volcanism (e.g., Fisher et al., 2017; Siegler et al., 2011), the latter of which may have created a transient atmosphere (Needham and Kring, 2017). In contrast, the main sources of volatiles trapped in crater PSRs that formed ≤ 3 Ga ago are solar wind and sporadic impact events. The smallest PSRs, like those potentially existing on the rim of Shackleton crater in the immediate vicinity of the south pole, are small and must be young. In those cases, any trapped volatiles should be dominated by solar wind (Kring, 2019).

3.4. Limits imposed by topography and slope

Changes in elevation and the magnitude of slope may limit access to sample sites in the south polar region. To illustrate potential challenges, the topography along the rim of Shackleton crater and the nearby "Connecting Ridge" (after Gläser et al., 2014) is shown in Fig. 8, using data compiled in topographic maps of the region (e.g., Harish et al., 2019; McCanaan et al., 2019). The ridge that abuts Shackleton's rim rises to a total elevation of ~1900 m, or ~600 m above the south pole. If a crew landed at the south pole and had a walking EVA towards the lunar far side along the rim of Shackleton crater (beginning at the south pole, B, and continuing toward X in Fig. 8a), that would require an initial climb of ~140 m over a horizontal distance of 2 km. If the crew walked along the rim crest to the highest elevation in that section of the rim (~7 km from the south pole, along B to X in Fig. 8a), that would require a climb of ~470 m.

Please cite this article as: A. J. Gawronska, N. Barrett, S. J. Boazman et al., Geologic context and potential EVA targets at the lunar south pole, Advances in Space Research, https://doi.org/10.1016/j.asr.2020.05.035

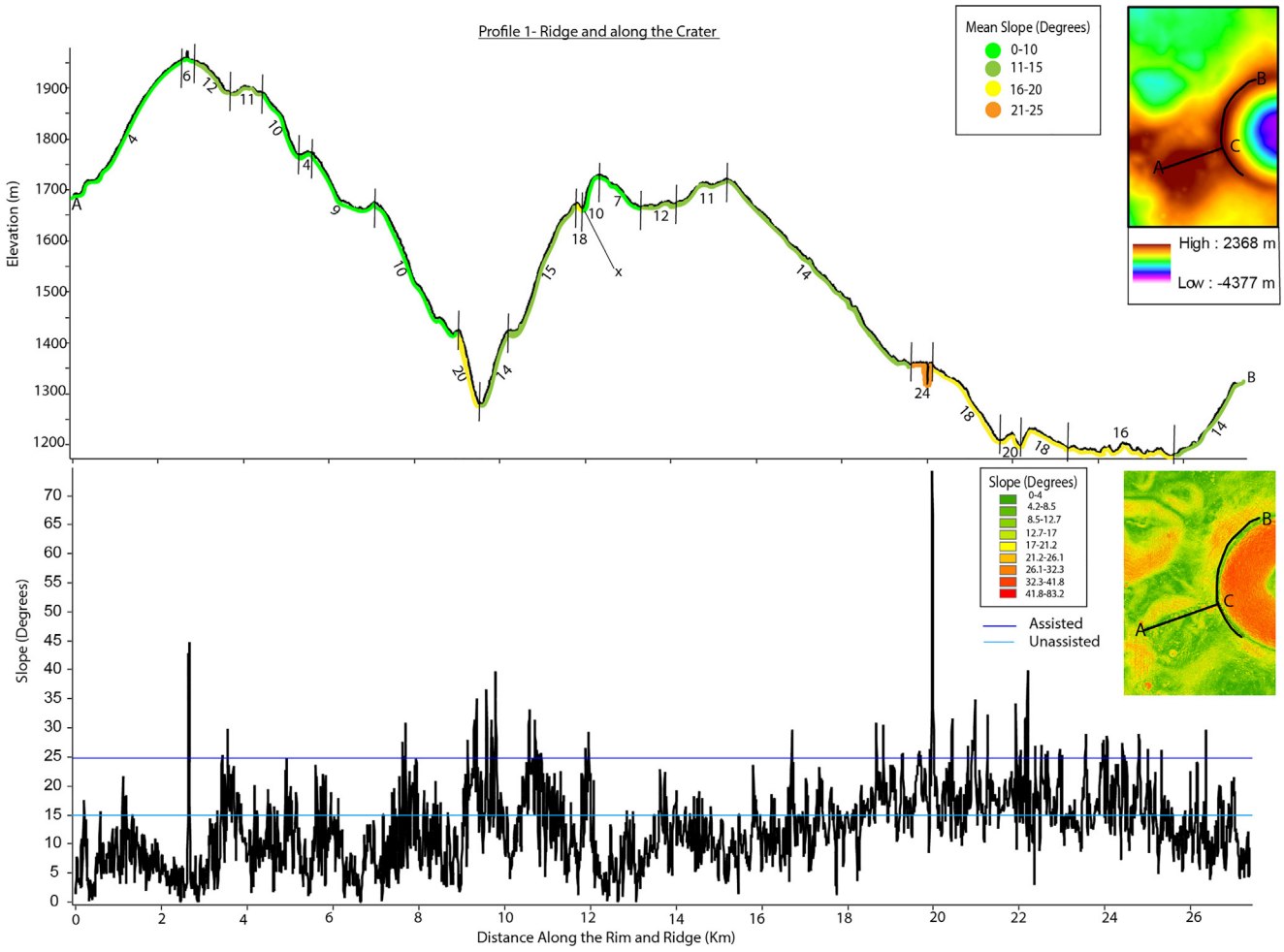

Fig. 8a. **Top:** Elevation profile (A-B) along the ridge that extends from Shackleton towards de Gerlache crater, and along Shackleton's rim, with the mean slope highlighted along the profile. The length of the traverse is ~27 km. **Bottom:** The variation in slope, highlighting the approximate limits of unassisted and rover-assisted crew along the A-B profile.

The slope along route A to B in Fig. 8a varies dramatically on the scale of 5 m/pixel, which represents variability imposed by heterogeneities in the Shackleton ejecta (e.g., Figs. 4–6) and small craters that now cover that ejecta (Fig. 8a, bottom panel). Average slopes are often tractable (e.g., ranging from 0° to 15°; Fig. 8a, top panel), although there remain zones with slope in excess of 15°. Slope is also variable farther along the rim of Shackleton crater (C to D in Fig. 8b). The average slope along the rim from the south pole to the ridge is 14.3° (over a distance of approximately 15 km; point B to X in Fig. 8a), and the average slope along the ridge is 10.6° (over a distance of approximately 12 km; point A to X in Fig. 8a). Detailed analysis of how these topographical changes correspond to lithological units near the Shackleton crater will further aid landing site selection (i.e., Ivanov et al., 2015a; 2015b).

4. Conclusions

Recent modeling suggests that the 4.1 km deep, 21 km diameter Shackleton crater was likely excavated by an ~1.5 km chondrite-like asteroid impacting a gabbroic anorthositic target with a velocity of ~15 km/s (Halim et al., under review). The resulting ejecta deposit presents many scientifically intriguing features for sampling during EVA. Such samples will be conducive to interpreting the geology of the lunar south pole (e.g., Fig. 9). The high albedo EVA targets described here likely, at least in part, correspond to the PAN units identified in the walls of Shackleton crater (Haruyama et al., 2008, 2013; Yamamoto et al., 2012). Numerous boulders and rock exposures in the region make sampling this high albedo material possible. The sizes of some of the exposures (up to 200 m) are far larger than anything sampled during the Apollo program and provide an opportunity to assess magmatic relationships within crystalline crustal units. Dark material of likely different composition exists inside the Shackleton crater wall and may also be present outside of the crater. Additional analysis regarding the distribution of these boulders would provide context regarding the location of rocky terrains, as well as regions with great sampling potential (i.e., Ivanov et al., 2015a, 2015b).

Please cite this article as: A. J. Gawronska, N. Barrett, S. J. Boazman et al., Geologic context and potential EVA targets at the lunar south pole, Advances in Space Research, https://doi.org/10.1016/j.asr.2020.05.035

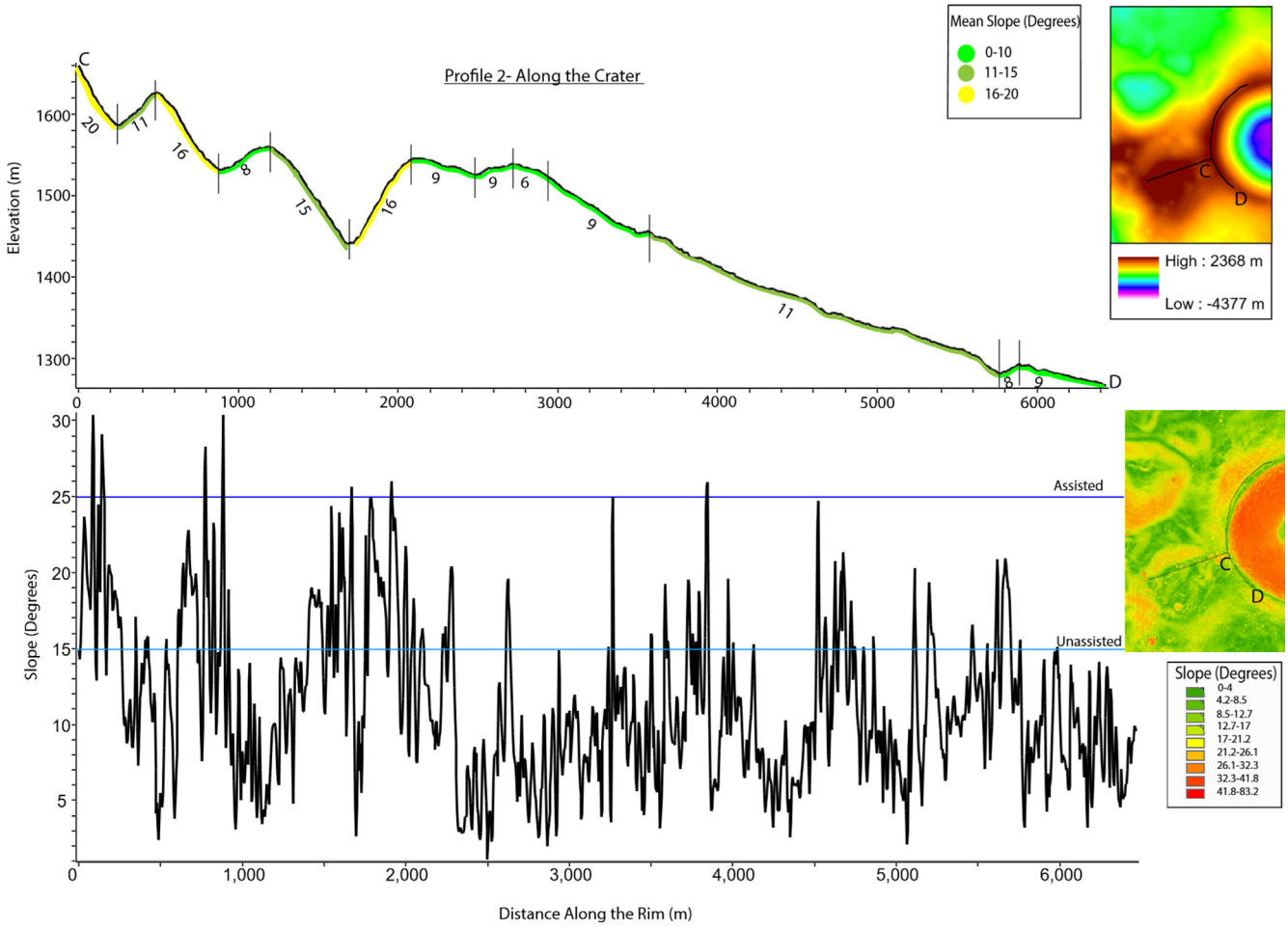

Fig. 8b. **Top:** Elevation profile (C-D) along Shackleton's rim with mean slope highlighted along the profile. This marks the continuation of traverse B-X from Fig. 8a. **Bottom:** The variation in slope highlighting the approximate limits of unassisted and rover-assisted EVAs.

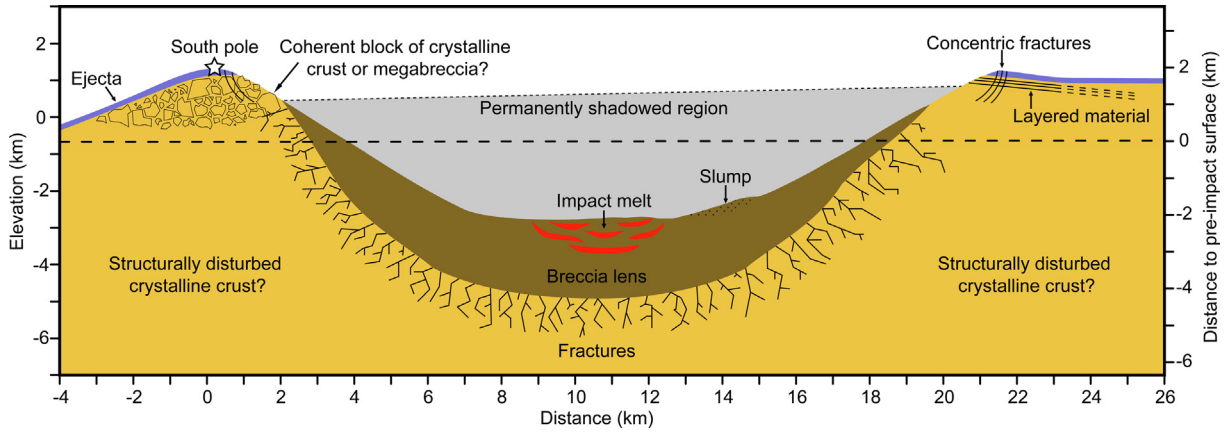

Fig. 9. Cross section summarizing the geology interpreted to exist in the Shackleton crater based on the findings of this study. The crater is approximately 4.1 km deep with respect to the rim and there is some slumping in the crater center (e.g., Zuber et al., 2012). Impact melt is believed to have mostly remained within the crater (Halim et al., under review). Concentric fractures surround the crater. Material exposed in the crater wall beneath the south pole may be exposed crust, or a megabreccia, while material exposed on the opposite crater wall appears layered. Due to the Shackleton PSR, it was not possible to determine the extent of either lithology. The ejecta surrounding Shackleton crater are modeled to be approximately 150 m in thickness (Halim et al., under review).

Please cite this article as: A. J. Gawronska, N. Barrett, S. J. Boazman et al., Geologic context and potential EVA targets at the lunar south pole, Advances in Space Research, https://doi.org/10.1016/j.asr.2020.05.035

A layered terrain occurs on the side of Shackleton crater opposite to the south pole and is exposed in the upper crater wall. These layers appear to be ejecta deposits of surrounding craters; the velocity of this ejecta landing at the Shackleton site is approximately 1000 km/hr. Ballistic sedimentation at these velocities likely caused mixing of ejecta with underlying material (Oberbeck, 1975). Since the Shackleton impact event also appears to have excavated layers of debris from pre-Nectarian and Nectarian craters, additional crustal components from more distant locales may also be available. Impact melts from those older craters (including the SPA basin) and from the host crater, Shackleton, may provide impact ages for deciphering the collisional modification of the ancient Moon. Additional sampling of the numerous PSRs existing near the lunar south pole (e.g., Cisneros et al., 2018; Mazarico et al., 2011) will address questions regarding the extent of volatile-bearing material. Sampling PSRs will provide an opportunity to assess the composition, extent, depth, and volume of volatiles, which may be used for future sustainable exploration and ISRU initiatives (e.g., Crawford, 2015; Fegley and Swindle, 1993; Lawrence, 2016; Nozette et al., 2001; NRC, 2007).

Regolith along the rim and flanks of Shackleton can be used to evaluate regolith processes in a polar terrain. Volatiles mixed with that regolith may provide an important assessment of volatiles available for ISRU and scientific investigations. Sampling of both the regolith and possible rocks originating from the PAN unit is also necessary to expand our understanding of the geology of Shackleton crater and the cross-cutting massif, as well as the extent and geology of the SPA basin itself. Samples collected near the south pole will thus address questions regarding the lunar magma ocean hypothesis and the subsequent evolution of the crust in this region with respect to both magmatism and impact cratering. As defined by the parameters set by the Apollo program, many of the EVA targets presented here require rover assistance to access due to the complex topography of the region. Rover-assisted EVAs would allow astronauts to traverse steeper slopes, while pressurized rovers may allow access to distant areas of interest, creating more opportunities to sample a diverse suite of materials.

Acknowledgments

We thank Dr. Satoru Yamamoto for sharing the coordinates of PAN locations from Yamamoto et al. (2012) with our team. We also thank the staff of the Lunar and Planetary Institute for their support during an Exploration Science internship through the Center for Lunar Science and Exploration, where this work was completed. This work was supported by NASA Solar System Exploration Research Virtual Institute contracts NNA14AB07A and 80NSSC20M0016. This is LPI Contribution 2364. We greatly appreciate the detailed and constructive feedback from associate editor Dr. Anil Bhardwaj, as well as Dr. James Head III and an anonymous reviewer, regarding the work presented here.

Appendix A

Table A1 summarizes information regarding figures which are included in this article. Specifically, the table gives the approximate locations of features of interest described in the article, as well as the LROC NAC images used. The chosen NAC images were processed and projected to a lunar polar stereographic projection using the Integrated Software for Imagers and Spectrometers 3 (ISIS3) software. ArcMap (Esri GIS Software) was then utilized to extract latitude and longitude locations of the selected features, which are summarized in Table A1. Depending on the NAC images used, the exact locations of features may change; therefore, the reported latitude and longitude coordinates mark the center of the figure, and the NAC ID used is reported.

Table A1
Coordinates of features shown in Figs. 4–6, as well as the corresponding LROC NAC image IDs. The latitude and longitude coordinates are associated with the central point of each detailed figure.

Figure	Latitude	Longitude	NAC ID
4.d	−89.9765422	−87.10242849	M140136780R
4.e	−89.9462384	26.13427658	M140197843L
4.f	−89.94757671	−114.5614797	M140136780R
4.g	−89.95435969	−13.51230667	M140184301L
4.h	−89.94010469	34.00804208	M144858987R
5.d	−89.81342487	2.856443066	M140197843R
5.e	−89.88772889	−131.5191484	M140136780L
5.f	−89.8099088	−137.5508604	M140068959L
5.g	−89.74912978	57.90521551	M147253633L
5.h	−89.91433565	−122.862614	M140136780L
5.i	−89.89296881	24.55097003	M140197843R/L
6.d	−89.59289223	−153.5620435	M133799601R
6.e	−89.50555066	−177.5697388	M143766500R

References

Allender, E.J., Orgel, C., Almeida, N.V., Cook, J., Ende, J.J., Kamps, O., Mazrouei, S., Slezak, T.J., Soini, A.-J., Kring, D.A., 2019. Traverses for the ISECG-GER design reference mission for humans on the lunar surface. Adv. Space Res. 63, 692–727. https://doi.org/10.1016/j.asr.2018.08.032.

Anand, M., 2010. Lunar water: A brief review. Earth Moon Planet. 107, 65–73. https://doi.org/10.1007/s11038-010-9377-9.

Anand, M., Crawford, I.A., Balat-Pichelin, M., Abanades, S., van Westrenen, W., Péraudeau, G., Jaumann, R., Seboldt, W., 2012. A brief review of chemical and mineralogical resources on the Moon and their potential utilization. Planet. Space Sci. 74 (1), 42–48. https://doi.org/10.1016/j.pss.2012.08.012.

ArcGIS [GIS software]. Version 10.0. Redlands, CA: Environmental Systems Research Institute, Inc., 2010.

Arnold, J.R., 1979. Ice in the lunar polar regions. J. Geophys. Res. 84, 5659–5668. https://doi.org/10.1029/JB084iB10p05659.

Basilevsky, A.T., Head III, J.W., Horz, F., Ramsley, K., 2015. Survival times of meter-sized rock boulders on the surface of airless bodies. Planet. Space Sci. 117, 312–328. https://doi.org/10.1016/j.pss.2015.07.003.

Basilevsky, A.T., Krasilnikov, S.S., Ivanov, M.A., Malenkov, M.A., Michael, G.G., Liu, T., Head, J.W., Scott, D.R., Lark, L., 2019. Potential lunar base on mons malapert: topographic, geologic and trafficability considerations. Sol. Syst. Res. 53 (5), 383–398. https://doi.org/10.1134/S0038094619050022.

Bickel, V.T., Honniball, C.I., Martinez, S.N., Rogalski, A., Sargeant, H. M., Bell, S.K., Czaplinski, E.C., Farrant, B.E., Harrington, E.M., Tolometti, G.D., Kring, D.A., 2019. Analysis of lunar boulder tracks: implications for trafficability of pyroclastic deposits. J. Geophys. Res. Planets 124, 1–19. https://doi.org/10.1029/2018JE005876.

Borst, A.M., Foing, B.H., Davies, G.R., van Westrenen, W., 2012. Surface mineralogy and stratigraphy of the lunar South Pole-Aitken basin determined from Clementine UV/VIS and NIR data. Planet. Space Sci. 68, 76–85. https://doi.org/10.1016/j.pss.2011.07.020.

Bridenstine, J., 2019. The scientific context for the exploration of the moon. NASA Release, 19-022.

Campbell, D.B., Campbell, B.A., Carter, L.M., Luc-Margot, J., Stacy, N.J.S., 2006. No evidence for thick deposits of ice at the lunar south pole. Nature 443, 835–837. https://doi.org/10.1038/nature0516745.

Chapman, C.R., Cohen, B.A., Grinspoon, D.H., 2007. What are the real constraints on the existence and magnitude of the late heavy bombardment?. Icarus 189, 233–245. https://doi.org/10.1016/j.icarus.2006.12.020.

Chin, G., Brylow, S., Foote, M., Garvin, J., Kasper, J., Keller, J., Litvak, M., Mitrofanov, I., Page, D., Raney, K., Robinson, M., Sanin, A., Smith, D., Spence, H., Spudis, P., Stern, S.A., Zuber, M., 2007. Lunar reconnaissance orbiter overview: the instrument suite and mission. Space Sci. Rev. 129 (4), 391–419. https://doi.org/10.1007/s11214-007-9153-y.

Cisneros, E., Boyd, A.K., Brown, H.M., Awumah, A.A., Martin, A.C., Paris, K.N., Leland, J., Povilaitis, R.Z., Hoppe, R., Davis, L.M., Estes, N.M., Robinson, M.S., and the LROC Team, 2018. Lunar Reconnaissance Orbiter Camera: Permanently Shadowed Regions Atlas. http://lroc.sese.asu.edu/psr.

Cohen, B.A., Swindle, T.D., Kring, D.A., 2000. Support for the lunar cataclysm hypothesis from lunar meteorite impact melt ages. Science 290, 1754–1756. https://doi.org/10.1126/science.290.5497.1754.

Colaprete, A., Schultz, P., Heldmann, J., Wooden, D., Shirley, M., Ennico, K., Hermalyn, B., Marshall, W., Ricco, A., Elphic, R.C., Goldstein, D., Summy, D., Bart, G.D., Asphaug, E., Korycansky, D., Landis, D., Sollitt, L., 2010. Detection of water in the LCROSS ejecta plume. Science 33 (6003), 463–468. https://doi.org/10.1126/science.1186986.

Connolly, J.F., 2006. Constellation program overview. NASA Constellation Program Office, Washington, DC.

Crawford, I.A., 2015. Lunar resources: A review. Prog. Phys. Geogr. 39 (2), 137–167. https://doi.org/10.1177/0309133314567585.

Ćuk, M., 2012. Chronology and sources of lunar impact bombardment. Icarus 218, 69–79. https://doi.org/10.1016/j.icarus.2011.11.031.

Daubar, I.J., Atwood-Stone, C., Byrne, S., McEwen, A.S., Russell, P.S., 2014. The morphology of small fresh craters on Mars and the Moon. J. Geophys. Res. 119, 2620–2639. https://doi.org/10.1002/2014JE004671.

Day, B., Law, E., 2018. NASA's Moon Trek: Extending capabilities for lunar mapping and modeling. 42nd COSPAR Scientific Assembly, Abstract id. B3.1-11-18.

Deutsch, A.N., Head III, J.W., Neumann, G.A., 2020. Analyzing the ages of south polar craters on the Moon: Implications for the sources and evolution of surface water ice. Icarus 336 (15). https://doi.org/10.1016/j.icarus.2019.113455 113455.

Duke, M.B., Blair, B.R., Diaz, J., 2003. Lunar resource utilization: implications for commerce and exploration. Adv. Space Res. 31 (11), 2413–2419. https://doi.org/10.1016/80273-1177(03)00550-7.

Edmundson, K.L., Cook, D.A., Thomas, O.H., Archinal, B.A., Kirk, R. L., 2012. Jigsaw: The ISIS3 bundle adjustment for extraterrestrial photogrammetry. Int. Ann. Photogrammetry, Remote Sens., Spatial Inf. Sci. I-4, 203–208. https://doi.org/10.5194/isprsannals-I-4-203-2012.

Edwards, K., 1987. Geometric processing of digital images of the planets. Photogramm. Eng. Remote Sens. 53 (9), 1219–1222.

Fassett, C.I., Head, J.W., Kadish, S.J., Mazarico, E., Neumann, G.A., Smith, D.E., Zuber, M.T., 2012. Lunar impact basins: Stratigraphy, sequence and ages rom superposed impact crater populations measures from Lunar Orbiter Laser Altimeter (LOLA) data. J. Geophys. Res. 117, E00H06. https://doi.org/10.1029/2011JE003951.

Fassett, C.I., Minton, D.A., 2013. Impact bombardment of the terrestrial planets and the early history of the Solar System. Nat. Geosci. 6, 520–524. https://doi.org/10.1038/ngeo1841.

Fegley, B., Swindle, T.D., 1993. Lunar volatiles: Implications for lunar resource utilization. In: Lewis, J., Matthews, M.S., Guerieri, M.L. (Eds.), Resources of Near Earth Space. Tucson University Press, Tucson, AZ, pp. 367–426.

Feldman, W.C., Maurice, S., Lawrence, D.J., Little, R.C., Lawson, S.L., Gasnault, , Wiens, R.C., Barraclough, B.L., Elphic, R.C., Prettyman, T.H., Steinberg, J.T., Binder, A.B., 2001. Evidence for water ice near the lunar poles. J. Geophys. Res. Planets 106 (E10), 23231–23251. https://doi.org/10.1029/2000JE001444.

Fisher, E.A., Lucey, P.G., Lemelin, M., Greenhagen, B.T., Siegler, M.A., Mazarico, E., Aharonson, O., Williams, J.-P., Hayne, P.O., Neumann, G.A., Paige, D.A., Smith, D.E., Zuber, M.T., 2017. Evidence for surface water ice in the lunar polar regions using reflectance measurements from the Lunar Orbiter Laser Altimeter and temperature measurements from the Diviner Lunar Radiometer Experiment. Icarus 292, 74–85. https://doi.org/10.1016/j.icarus.2017.03.023.

Flahaut, J., Carpenter, J., Williams, J.-P., Anand, M., Crawford, L.A., van Westrenen, W., Füri, E., Xiao, L., Zhao, S., 2020. Regions of interest (ROI) for future exploration missions to the lunar South Pole. Planet. Space Sci. 180, 1–15. https://doi.org/10.1016/j.pss.2019.104750.

Fortezzo, C.M., Spudis, P.D., Harrel, S.L., 2020. Release of the digital unified global geologic map of the moon At 1:5,000,000-scale. Paper presented at the 51st Lunar and Planetary Science Conference, Lunar and Planetary Institute, Houston, TX. https://www.hou.usra.edu/meetings/lpsc2020/pdf/2760.pdf.

Gladstone, G.R., Stern, S.A., Retherford, K.D., Black, R.K., Slater, D.C., Davis, M.W., Versteeg, M.H., Persson, K.B., Parker, J.W., Kaufmann, D.E., Egan, A.F., Greathouse, T.K., Feldman, P.D., Hurley, D., Pyor, W.R., Hendrix, A.R., 2010. LAMP: the lyman alpha mapping project on NASA's lunar reconnaissance orbiter mission. Space Sci. Rev. 150, 161–181. https://doi.org/10.1007/s11214-009-9578-6.

Gladstone, G.R., Retherford, K.D., Egan, A.F., Kaufmann, D.E., Miles, P.F., Parker, J.W., Horvath, D., Rojas, P.M., Versteeg, M.H., Davis, M.W., Greathouse, T.K., Slater, D.C., Mukherjee, J., Steffl, A.J., Feldman, P.D., Hurley, D.M., Pryor, W.R., Hendrix, A.R., Mazarico, E., Stern, S.A., 2012. Far-ultraviolet reflectance properties of the Moon's permanently shadowed regions. J. Geophys. Res.: Planets 117 E12, E00H04. https://doi.org/10.1029/2011JE003913.

Gläser, P., Scholten, F., De Rosa, D., Figuera, R.M., Oberst, J., Mazarico, E., Neumann, G.A., Robinson, M.S., 2014. Illumination conditions at the lunar south pole using high resolution digital terrain models from LOLA. Icarus 243, 78–90. https://doi.org/10.1016/j.icarus.2014.08.013.

Gold, T., 1955. The lunar surface. MNRAS 155, 585–604.

Goswami, J.N., Annadurai, M., 2009. Chandrayaan-1: India's first planetary science mission to the Moon. Curr. Sci. 96 (4), 486–491.

Gruener, J.E., 2009. NASA constellation program office regions of interest on the moon. 2009 Annual Meeting of the Lunar Exploration and Analysis Group. https://www.lpi.usra.edu/meetings/leag2009/presentations/Day-2%20PM/03-35_Gruener.pdf.

Halim, S.H., Barrett, N., Boazman, S.J., Gawronska, A.J., Gilmour, C. M., Harish, McCanaan, K., Satyakumar, A. V., Shah, J., Kring, D., Under review. Numerical modelling of the formation of Shackleton crater at the lunar south pole. Submitted to Icarus.

Harish, Animireddi, V.S.K., Barrett, N., Boazman, S., Gawronska, A., Gilmour, C., Halim, S., McCanaan, K., Shah, J., Kring, D., 2019. Slope Map between Shackleton and de Gerlache Craters, Lunar South

Please cite this article as: A. J. Gawronska, N. Barrett, S. J. Boazman et al., Geologic context and potential EVA targets at the lunar south pole, Advances in Space Research, https://doi.org/10.1016/j.asr.2020.05.035

Pole, Map 1. LPI Lunar South Pole Atlas, LPI Contribution #2227, https://hdl.handle.net/20.500.11753/1360.

Hartmann, W.K., 2003. Megaregolith evolution and cratering cataclysm models – Lunar cataclysm as a misconception (28 years later). Meteorit. Planet. Sci. 38 (4), 579–593. https://doi.org/10.1111/j.1945-5100.2003.tb00028.x.

Hartmann, W.K., 2019. History of the terminal cataclysm paradigm: epistemology of a planetary bombardment that never (?) happened. Geosciences 9 (7), 285. https://doi.org/10.3390/geosciences9070285.

Haruyama, J., Ohtake, M., Matsunaga, T., Morota, T., Honda, C., Yokota, Y., Pieters, C.M., Hara, S., Hioki, K., Saiki, K., Miyamoto, H., Iwasaki, A., Abe, M., Ogawa, Y., Takeda, H., Shirao, M., Yamaji, A., Josset, J.-L., 2008. Lack of exposed ice inside lunar south pole shackleton crater. Science 322 (5903), 938–939. https://doi.org/10.1126/science:1164020.

Haruyama, J., Yamamoto, S., Yokota, Y., Ohtake, M., Matsunaga, T., 2013. An explanation of bright areas inside Shackleton Crater at the Lunar South Pole other than water-ice deposits. Geophys. Res. Lett. 40 (15), 3814–3818. https://doi.org/10.1002/grl.50753.

Hayne, P.O., Hendrix, A., Sefton-Nash, E., Siegler, M.A., Lucey, P.G., Retherford, K.D., Paige, D.A., 2015. Evidence for exposed water ice in the Moon's south polar regions from Lunar Reconnaissance Orbiter ultraviolet albedo and temperature measurements. Icarus 255, 58–69. https://doi.org/10.1016/j.icarus.2015.03.032.

Hiesinger, H., Head, J.W., Wolf, U., Jaumann, R., Neukum, G., 2011. In: Ambrose, W.A., Williams, D.A. (Eds.), Recent Advances and Current Research Issues in Lunar Stratigraphy, 477. Geological Society of America Special PaperThe Geological Society of America Inc, Boulder, CO, pp. 1–51. https://doi.org/10.1130/2011.2477(01).

Hiesinger, H., Van der Bogert, C.H., Pasckert, J.H., Funcke, L., Giacomini, L., Ostrach, L.R., Robinson, M.S., 2012. How old are young lunar craters? J. Geophys. Res. Planets 117, E00H10. https://doi.org/10.1029/2011JE003935.

Hurwitz, D., Kring, D.A., 2015. Potential sample sites for South Pole-Aitken basin impact melt within the Schrodinger basin. Earth Planet. Sci. Lett. 427, 31–36. https://doi.org/10.1016/j.epsl.2015.06.055.

Ivanov, M.A., Basilevsky, A.T., Abdrakhimov, A.M., Karachevtseva, I. P., Kohanov, A., Head III, J.W., 2015a. Boguslawsky crater on the Moon: Geology and assessment of the boulder distribution on its floor. Astronomicheskii Vestnik 49, 403–419. https://doi.org/10.7868/S0320930X15060031.

Ivanov, M.A., Hiesinger, H., Abdrakhimov, A.M., Basilevsky, A.T., Head III, J.W., Pasckert, J.H., Bauch, K., van der Bogert, C.H., Gläser, P., Kohanov, A., 2015b. Landing site selection for Luna-Glob mission in crater Boguslawsky. Planet. Space Sci. 117, 45–63. https://doi.org/10.1016/j.pss.2015.05.007.

James, P.B., Smith, D.E., Byrne, P.K., Kendall, J.D., Melosh, H.J., Zuber, M.T., 2019. Deep structure of the lunar south pole-Aitken basin. Geophys. Res. Lett. 46, 1–7. https://doi.org/10.1029/2019/GL082252.

Jawin, E.R., Valencia, S.N., Watkins, R.N., Crowell, J.M., Neal, C.R., Schmidt, G., 2019. Lunar science for landed missions workshop findings report. Earth Space Sci. 6. https://doi.org/10.1029/2018EA000490.

Kramer, G.Y., Kring, D.A., Nahm, A.L., Pieters, C.M., 2013. Spectral and photogeologic mapping of Schrödinger Basin and implications for post-south Pole-Aitken impact deep subsurface stratigraphy. Icarus 223, 131–148. https://doi.org/10.1016/j.icarus.2012.11.008.

Kring, D.A., 1995. The dimensions of the Chicxulub impact crater and impact melt sheet. J. Geophys. Res. 100, 16979–16986. https://doi.org/10.1029/95JE01768.

Kring, D.A., 2007. Guidebook to the Geology of Barringer Meteorite Crater, Arizona, Lunar and Planetary Institute, Houston, TX, 150 pp. (LPI Contribution Number 1355).

Kring, D.A., 2017. Guidebook to the Geology of Barringer Meteorite Crater, Arizona (aka Meteor Crater) Second edition, Lunar and Planetary Institute, Houston, TX, 272 pp. (LPI Contribution Number 2040).

Kring, D.A., 2019. Lunar South Pole Geology: Preparing for a Seventh Lunar Landing. NASA Exploration Science Forum 2019. NASA Ames Research Center, Moffett Field, CA. July 23 – 25, 2019. SSERVI ID: NESF2019-127.

Landau, Elizabeth. "Artemis Moon Program Advances – The Story So Far." Edited by Thalia Patrinos, NASA, NASA, 31 May 2019, www.nasa.gov/artemis-moon-program-advances.

Lawrence, D.J., 2016. A tale of two poles: Toward understanding the presence, distribution, and origin of volatiles at the polar regions of the Moon and Mercury. J. Geophys. Res. Planets 122, 21–52. https://doi.org/10.1002/2016JE005167.

Lemelin, M., Blair, D.M., Roberts, C.E., Runyon, K.D., Nowka, D., Kring, D.A., 2014. High-priority lunar landing sites for in situ and sample return studies of polar volatiles. Planet. Space Sci. 101, 149–161. https://doi.org/10.1016/j.pss.2014.07.002.

Lemelin, M., Lucey, P.G., Song, E., Taylor, G.J., 2015. Lunar central peak mineralogy and iron content using th Kaguya Multiband Imager: Reassessment of the compositional structure of lunar crust. J. Geophys. Res. Planets 120 (5), 869–887. https://doi.org/10.1002/2014JE004778.

Lewis, R., Toups, L., Hoffman, S., Gruener, J., Jagge, A., Deitrick, S., Hinterman, E., Lawrence, S., 2019. Site planning and design to enable lunar and Mars human exploration. Annual Meeting of the Lunar Exploration Analysis Group (LEAG), Abstract #5062.

Li, S., Lucey, P.G., Miliken, R.E., Hayne, P.O., Fisher, E., Williams, J.-P., Hurely, D.M., Elphic, R.C., 2018. Direct evidence of surface exposed water ice in the lunar polar regions. Proc. Natl. Acad. Sci. 115, 201802345. https://doi.org/10.1073/pnas.1802345115.

Longhi, J., 2003. A new view of lunar ferroan anorthosites: Postmagma ocean petrogenesis. J. Geophys. Res. Planets 108 (E8), 2–11. https://doi.org/10.1029/2002JE001941.

Mandt, K.E., Greathouse, T.K., Retherford, K.D., Gladstone, G.R., Jordan, A.P., Lemelin, M., Koeber, S.D., Bowmna-Cisneros, E., Patterson, G.W., Robinson, M., Lucey, P.G., Hendrix, A.R., Hurley, D., Strickle, A.M., Pryor, W., 2016. LRO-LAMP detection of geologically young craters within lunar permanently shadowed regions. Icarus 273, 114–120. https://doi.org/10.1016/j.icarus.2015.07.031.

Marchi, S., Bottke, W.F., Kring, D.A., Morbidelli, A., 2012. The onset of lunar cataclysm as recorded in its ancient crater populations. Earth Planet. Sci. Lett. 325–326, 27–28. https://doi.org/10.1016/j.epsl.2012.01.021.

Mazarico, E., Neumann, G.A., Smith, D.E., Zuber, M.T., Torrence, M. H., 2011. Illumination conditions of the lunar polar regions using LOLA topography. Icarus 211, 1066–1081. https://doi.org/10.1016/j.icarus.2010.10.030.

McCanaan, K., Animireddi, V.S.K., Barrett, N., Boazman, S., Gawronska, A., Gilmour, C., Halim, S., Harish, Shah, J., Kring, D., 2019. Slope Map of the Moon's South Pole Ridge. LPI Lunar South Pole Atlas, LPI Contribution #2214.

Miller, R.S., Lawrence, D.J., Hurley, D.M., 2014. Identification of surface hydrogen enhancements within the Moon's Shackleton Crater. Icarus 233, 229–232. https://doi.org/10.1016/j.icarus.2014.02.007.

Mitrofanov, L.G., Bartels, A., Bobrovnitsky, Y.I., Boynton, W., Chin, G., Enos, H., Evans, L., Floyd, S., Garvin, J., Golovin, D.V., Grebennikov, A.S., Harshman, K., Kazakov, L.L., Keller, J., Konovalov, A. A., Kozyrev, A.S., Krylov, A.R., Litvak, M.L., Malakhov, A.V., McClanahan, T., Milikh, G.M., Mokrousov, M.I., Ponomareva, S., Sagdeev, R.Z., Sanin, A.B., Shevchenko, V.V., Shvetsov, V.N., Starr, R., Timoshenko, G.N., Tomilina, T.M., Tretyakov, V.I., Trombka, J., Troshin, V.S., Uvarov, V.N., Varennikov, A.B., Vostrukhin, A.A., 2010a. Lunar exploration neutron detector for the NASA lunar reconnaissance orbiter. Space Sci. Rev. 150, 183–207. https://doi.org/10.1007/s11214-009-9608-4.

Mitrofanov, I.G., Sanin, A.B., Boynton, W.V., Chin, G., Garvin, J.B., Golovin, D., Evans, L.G., Harshman, K., Kozyrev, A.S., Litvak, M. L., Malakhov, A., Mazarico, E., McClanahan, T., Milikh, G., Mokrousov, M., Nandikotkur, G., Neumann, G.A., Nuzhdin, I., Sgdeev, R., Shevchenko, V., Shvetsov, V., Smith, D.E., Starr, R.,

Tretyakov, V.I., Trombka, J., Usikov, D., Varenikov, A., Vostrukhin, A., Zuber, M.T., 2010b. Hydrogen mapping of the lunar south pole using the LRO neutron detector experiment LEND. Science 330 (6003), 483–486. https://doi.org/10.1126/science.1185696.

Moore, H.J., Boyce, J.M., Hahn, D.A., 1980. Small impact craters in the lunar regolith – Their morphologies, relative ages, and rates of formation. Earth Moon Planet. 23 (2), 231–252. https://doi.org/10.1007/BF00899820.

Morbidelli, A., Marchi, Bottke, W.F., Kring, D.A., 2012. A sawtooth-like timeline for the first billion years of lunar bombardment. Earth Planet. Sci. Lett. 355, 144–151. https://doi.org/10.1016/j.epsl.2012.07.037.

Moriarty III, D.P., Pieters, C.M., 2018. The character of south pole-aitken basin: patterns of surface and subsurface composition. J. Geophys. Res. Planets 123, 729–747. https://doi.org/10.1002/2017JE005364.

Nagaoka, H., Takeda, H., Karouji, Y., Ohtake, M., Yamaguchi, A., Yoneda, S., Hasebe, N., 2014. Implications for the origins of pure anorthosites found in the feldspathic lunar meteorites, Dhofar 489 group. Earth Planets Space 66, 115. https://doi.org/10.1186/1880-5981-66-115.

National Aeronautics and Space Administration (NASA), 2007. NASA Advisory Council Workshop on Science Associated with the Lunar Exploration Architecture. Tempe, AZ: CreateSpace Independent Publishing Platform, pp. 27–30.

National Aeronautics and Space Administration (NASA), Human Landing System Concept of Operations, V 1.0 Release candidate 1.3, September 24, 2019a.

National Aeronautics and Space Administration (NASA), White Paper: Initial Evaluation of Mission Design Sensitivity to Surface Stay Duration. August 28, 2019b.

National Research Council (NRC), 2007. The Scientific Context for Exploration of the Moon, Final Report, National Academy Press, Washington, D. C.

Needham, D., Kring, D.A., 2017. Lunar volcanism produced a transient atmosphere around the ancient Moon. Earth Planet. Sci. Lett. 478, 175–178. https://doi.org/10.1016/j.epsl.2017.09.002.

Noble, S.K., Pieters, C.M., Taylor, L.A., Morris, R.V., Allen, C.C., McKay, D.S., Keller, L.P., 2000. The optical properties of the finest fraction of lunar soil: Implications for space weathering. Meteorit. Planet. Sci. 36, 31–42. https://doi.org/10.1111/j.1945-5100.2001.tb01808.x.

Nozette, S., Spudis, P.D., Robinson, M.S., Bussey, D.B.J., Lichtenberg, C., Bonner, R., 2001. Integration of lunar polar remote-sensing data sets: Evidence for ice at the lunar south pole. J. Geophys. Res. 106 (10), 23253–23266. https://doi.org/10.1029/2000JE001417.

Oberbeck, V.R., 1975. The role of ballistic erosion and sedimentation in lunar stratigraphy. Rev. Geophys. Space Phys. 13 (2), 337–362. https://doi.org/10.1029/RG013i002p00337.

Ohtake, M., Haruyama, J., Matsunaga, T., Yokota, Y., Morota, T., Honda, C.LISM team, 2008. Performance and scientific objectives of the SELENE (KAGUYA) multiband imager. Earth Planets Space 60, 257–264.

Ohtake, M., Matsunaga, T., Haruyama, J., Yokota, Y., Morota, T., Honda, C., Ogawa, Y., Torii, M., Miyamoto, H., Arai, T., Hirata, N., Iwasaki, A., Nakamura, R., Hiroi, T., Sugihara, T., Takeda, H., Otake, H., Pieters, C.M., Saiki, K., Kitazato, K., Abe, M., Asada, N., Demura, H., Yamaguchi, Y., Sasaki, S., Kodama, S., Terazano, J., Shirao, M., Yamaji, A., Minami, S., Akiyama, H., Josset, J.-L., 2009. The global distribution of pure anorthosite on the Moon. Nature 461, 236–241. https://doi.org/10.1038/nature08317.

Öhmann, T., Kring, D.A., 2012. Phoogeologic analysis of impact melt-rich lithologies in Kepler crater that could be sampled by future missions. J. Geophys. Res. 117, E00H08. https://doi.org/10.1029/2011JE003918.

Paige, D.A., Siegler, M.A., Zhang, J.A., Hayne, P.O., Foote, E.J., Bennett, K.A., Vasavada, A.R., Greenhagen, B.T., Schofield, J.T., McCleese, D.J., Foote, M.C., DeJong, E., Bills, B.G., Hartford, W., Murray, B.C., Allen, C.C., Snook, K., Soderblom, L.A., Calcutt, S., Taylor, F.W., Bowles, N.E., Bandfield, J.L., Elphic, R., Ghent, R., Glotch, T.D., Wyatt, M.B., Lucey, P.G., 2010. Diviner lunar radiometer observations of cold traps in the Moon's south polar region. Science 330, 479–482. https://doi.org/10.1126/science.1187726.

Pieters, C.M., Tompkins, S., Head, J.W., Hess, P.C., 1997. Mineralogy of the mafic anomaly in the South Pole-Aitken Basin: Implications for excavation of the lunar mantle. Geophys. Res. Lett. 24 (15), 1903–1906. https://doi.org/10.1029/97GL01718.

Pieters, C.M., Head III, J.W., Gaddis, L., Jolliff, B., Duke, M., 2001. Rock types of South Pole-Aitken basin and extent of basaltic volcanism. J. Geophys. Res. 106 (E11), 28001–28022. https://doi.org/10.1029/2000JE001414.

Pieters, C., Head, J., Kring, D., Canup, R., Scott, D.R., 2018. Transformative Lunar Science. 42nd COSPAR Scientific Assembly B3.

Pike, R.J., 1974. Depth/diameter relations of fresh lunar craters: Revision from spacecraft data. Geophys. Res. Lett. 1 (7), 291–294. https://doi.org/10.1029/GL001i007p00291.

Potter, R.W.K., Collins, G.S., Kiefer, W.S., McGovern, P.J., Kring, D.A., 2012. Constraining the size of the South Pole-Aitken basin impact. Icarus 220, 730–743. https://doi.org/10.1016/j.icarus.2012.05.032.

Robinson, M.S., Brylow, S.M., Tschimmel, M., Humm, D., Lawrence, S.J., Thomas, P.C., Denevi, B.W., Bowman-Cisneros, E., Zerr, J., Ravine, M.A., Caplinger, M.A., Ghaemi, F.T., Schaffner, J.A., Malin, M.C., Mahanti, P., Bartels, A., Anderson, J., Tran, T.N., Eliason, E.M., McEwen, A.S., Turtle, E., Jolliff, B.L., Hiesinger, H., 2010. Lunar Reconnaissance Orbiter Camera (LROC) Instrument Overview. Space Sci. Rev. 150 (1–4), 81–124. https://doi.org/10.1007/s11214-010-9634-2.

Ryder, G., 2000. Glass beads tell a tale of lunar bombardment. Science 287, 1768–1769. https://doi.org/10.1126/science.287.5459.1768.

Sargeant, H., Bickel, V., Honniball, C.I., Martinez, S., Bell, S.K., Czaplinski, E.C., Rogaski, A., 2019. Determining the bearing capacity of permanently shadowed regions of the moon using boulder tracks. Lunar and Planetary Science Conference, Abstract #1792.

Schultz, P.H., Hermalyn, B., Colaprete, A., Enico, K., Shirley, M., Marshall, W.S., 2010. The LCROSS cratering experiment. Science 330 (6003), 468–472. https://doi.org/10.1126/science.1187454.

Siegler, M.A., Bills, B.G., Paige, D.A., 2011. Effects of orbital evolution on lunar ice stability. J. Geophys. Res. Planets 116 (E3), E03010. https://doi.org/10.1029/2010JE003652.

Siegler, M.A., Paige, D.A., Williams, J.-P., Bills, B., 2015. Evolution of lunar polar ice stability. Icarus 255, 78–87. https://doi.org/10.1016/j.icarus.2014.09.037.

Smith, D.E., Zuber, M.T., Neumann, G.A., Lemoine, F.G., Mazarico, E., Torrence, M.H., McGarry, J.F., Rowlands, D.D., Head III, J.W., Duxbury, T.H., Aharonsen, O., Lucey, P.G., Robinson, M.S., Barnouin, O.S., Cavanaugh, J.F., Sun, X., Liiva, P., Mao, D.-D., Smith, J.C., Bartels, A.E., 2010. Initial observations from the Lunar Orbiter Laser Altimeter (LOLA). Geophys. Res. Lett. 37, L18204. https://doi.org/10.1029/2010GL043751.

Speyerer, E.J., Robinson, M.S., 2013. Persistently illuminated regions at the lunar poles: Ideal sites for future exploration. Icarus 222 (1), 122–136. https://doi.org/10.1016/j.icarus.2012.10.010.

Spudis, P.D., 2011. The Moon: Port of Entry to Cislunar Space. In: Toward a Theory of Spacepower, National Defense University Press, Washington D. C.

Spudis, P.D., Lavoie, A.R., 2010. Mission and Implementation of an Affordable Lunar Return. Proceedings, Space Manufacturing 14, Space Studies Institute, Princeton NJ.

Spudis, P.D., Ryder, G., (Eds.), 1985. Workshop on the geology and petrology of the apollo 15 landing site. Lunar and Planetary Institute Technical Report 86-03, Lunar and Planetary Institute, Houston, Texas, 77068-4399.

Spudis, P.D., Bussey, B., Plescia, J., Josset, J.-L., Beauvivre, S., 2008. Geology of Shackleton Crater and the south pole of the Moon. Geophys. Res. Lett. 35, L14201. https://doi.org/10.1029/2008GL034468.

Stopar, J., Meyer, H., 2019. Topography and Permanently Shaded Regions (PSRs) of the Moon's South Polar Ridge. Lunar and

Please cite this article as: A. J. Gawronska, N. Barrett, S. J. Boazman et al., Geologic context and potential EVA targets at the lunar south pole, Advances in Space Research, https://doi.org/10.1016/j.asr.2020.05.035

Planetary Institute Regional Planetary Image Facility, LPI Contribution, p. 2178.

Stöffler, D., Ryder, G., Ivanov, B.A., Artemieva, N.A., Cintala, M.J., Grieve, R.A.F., 2006. Cratering history and lunar chronology. In: New Views of the Moon. Rev. Mineral. Geochem. 60 (1), 519–596. https://doi.org/10.2138/rmg.2006.60.05.

Swann, G.A., Bailey, N.G., Batson, R.M., Eggleton, R.E., Hait, M.H., Holt, H.E., Larson, K.B., Reed, V.S., Schaber, G.G., Sutton, R.L., Trask, N.J., Ulrich, G.E., Wilshire, H.G., 1977. Geology of the Apollo 14 Landing Site in the Fra Mauro Highlands. U. S. Geological Survey Professional Paper 880.

Tera, D., Papanastassiou, D.A., Wasserburg, G.J., 1974. Isotopic evidence for a terminal lunar cataclysm. Earth Planet. Sci. Lett. 22, 1–21. https://doi.org/10.1016/0012-821X(74)90059-4.

Thompson, T.W., Masursky, H., Shorthill, R.W., Tyler, G.L., Zisk, S.H., 1974. A comparison of infrared, radar, and geologic mapping of lunar craters. Earth Moon Planet. 10 (1), 87–117. https://doi.org/10.1007/BF00562019.

Thomson, B.J., Bussey, D.B.J., Neish, C.D., Cahill, J.T.S., Heggy, E., Kirk, R.L., Patterson, G.W., Raney, R.K., Spudis, P.D., Thompson, T.W., Ustinov, E.A., 2012. An upper limit for ice in Shackleton crater as revealed by LRO Mini-RF orbital radar. Geophys. Res. Lett. 39, L14201. https://doi.org/10.1029/2012GL05119.

Torson, J.M., 1989. Interactive image cube visualization and analysis. In: Proceedings of the 1989 Chapel Hill workshop on Volume visualization, May 1989, pp. 33–38.

Tye, A.R., Fassett, C.I., Head, J.W., Mazarico, E., Basilevsky, A.T., Neumann, G.A., Smith, D.E., Zuber, M.T., 2015. The age of lunar south circumpolar craters Haworth, Shoemaker, Faustini, and Shackleton: Implications for regional geology, surface processes, and volatile sequestration. Icarus 255, 70–77. https://doi.org/10.1016/j.icarus.2015.03.016.

Ulrich, G.E., Hodges, C.A., Muehlberger, W.R., 1981. Geology of the Apollo 16 Area. Central Lunar Highlands. U. S, Geological Survey Professional Paper, p. 1048.

Vaughan, W.M., Head, J.W., 2014. Impact melt differentiation in the South Pole-Aitken basin: Some observations and speculations. Planet. Space Sci. 91, 101–106. https://doi.org/10.1016/j.pss.2013.11.010.

Watson, K., Murray, B.C., Brown, H., 1961. The behavior of volatiles on the lunar surface. J. Geophys. Res. 66, 3033–3045. https://doi.org/10.1029/JZ066i009p03033.

Wieczorek, M.A., Jolliff, B.L., Khan, A., Pritchard, M.E., Weiss, B.P., Williams, J.G., Hood, L.L., Rigter, K., Neal, C.R., Shearer, C.K., McCallum, I.S., Tompkins, S., Hawke, B.R., Peterson, C., Gillis, J.J., Bussey, B., 2006. The constitution and structure of the lunar interior. Rev. Mineral. Geochem. 60 (1), 221–364. https://doi.org/10.2138/rmg.2006.60.3.

Wilhelms, D.E., 1987. Geologic history of the Moon, U. S. Geological Survey Professional Paper 1348, 302 pp.

Wilhelms, D.E., Howard, K.A., Wilshire, H.G., 1979. Geologic map of the south pole of the Moon, U. S. Geological Survey, Map, I-1162.

Wolfe, E.W., Bailey, N.G., Lucchitta, B.K., Muehlberger, W.R., Scott, D. H., Sutton, R.L., Wilshire, H.G., 1981. The Geologic Investigation of the Taurus-Littrow Valley: Apollo 17 Landing Site. U. S. Geological Survey Professional Paper 1080.

Yamamoto, S., Nakamura, R., Matsunaga, T., Ogawa, Y., Ishihara, Y., Morota, T., Hirata, N., Ohtake, M., Hiroi, T., Yokota, Y., Haruyama, J., 2012. Massive layer of pure anorthosite on the Moon. Geophys. Res. Lett. 39, L13201. https://doi.org/10.1029/2012GL052098.

Zuber, M.T., Head, J.W., Smith, D.E., Neumann, G.A., Mazarico, E., Torrence, M.H., Aharonson, O., Tye, A.R., Fassett, C.I., Rosenburg, M.A., Melosh, H.J., 2012. Constrains on the volatile distribution within Shackleton crater at the lunar south pole. Nature 486, 378–382. https://doi.org/10.1038/nature11216.

Please cite this article as: A. J. Gawronska, N. Barrett, S. J. Boazman et al., Geologic context and potential EVA targets at the lunar south pole, Advances in Space Research, https://doi.org/10.1016/j.asr.2020.05.035